Intercomparison of atmospheric Carbonyl Sulfide (TransCom-COS; Part one): Evaluating the impact of transport and emissions on tropospheric variability using ground-based and aircraft data

Marine Remaud[1], Jin Ma[2], Maarten Krol[2,3], Camille Abadie[1], Mike Cartwright[4,5], Prabir Patra[6], Yosuke Niwa[7,8], Christian Rodenbeck[9], Sauveur Belviso[1], Linda Kooijmans[3], Sinikka Lennartz[10], Fabienne Maignan[1], Martyn P. Chipperfield[11,12], Richard J. Pope[11,12], Jeremy J. Harrison[11,12], Christopher Wilson[11,12] and Philippe Peylin[1]

[1] Laboratoire des Sciences du Climat et de l'Environnement, CEA-CNRS-UVSQ, UMR 8212, IPSL, Gif-sur-Yvette, France

[2] Institute for Marine and Atmospheric Research, Utrecht University, Utrecht, the Netherlands

[3]Meteorology and Air Quality, Wageningen University and Research, Wageningen, the Netherlands

[4]School of Physics and Astronomy, Space Park Leicester, University of Leicester, Leicester, UK

[5]National Centre for Earth Observation, Space Park Leicester, University of Leicester, Leicester, UK

[6]Research Institute for Global Change, JAMSTEC, Yokohama 236-0001, Japan

[7]National Institute for Environmental Studies, 16-2 Onogawa, Tsukuba, Ibaraki, 305-8506, Japan

[8]Meteorological Research Institute, 1-1 Nagamine, Tsukuba, Ibaraki, 305-0052, Japan

[9]Max Planck Institute for Biogeochemistry, Jena, Germany

[10]Institute and Chemistry and Biology of the Marine Environment, University of Oldenburg, Oldenburg, Germany

[11]School of Earth and Environment, University of Leeds, Leeds, UK

[12]National Centre for Earth Observation, University of Leeds, Leeds, UK

Corresponding author: Marine Remaud (marine.remaud@lsce.ipsl.frr)

Key Points:

- The models-observation mismatch suggests there is a missing source in the tropics and a missing sink in the high northern latitude in summer.
- The model spread reaches 80 ppt at northern latitude sites in summer
- The diurnal rectifier effect does not exceed 30 ppt.

Abstract

We present a comparison of atmospheric transport model simulations for carbonyl sulfide (COS), within the framework of the ongoing atmospheric tracer transport model intercomparison project "TransCom". Seven atmospheric transport models participated in the inter-comparison experiment and provided simulations of COS mixing ratios in the troposphere over a 9-year period (2010–2018), using prescribed state-of-the-art surface fluxes for various components of the atmospheric COS budget: biospheric sink, oceanic source, sources from fire and industry. Since the biosphere is the largest sink of COS, we tested sink estimates produced by two different biosphere models. The main goals of TransCom-COS are (a) to investigate the impact of the transport uncertainty and emission distribution in simulating the spatio-temporal variability of COS mixing ratios in the troposphere, and (b) to assess the sensitivity of simulated tropospheric COS mixing ratios to the seasonal and diurnal variability of the COS biosphere fluxes. To this end, a control case with state-of-the-art seasonal fluxes of COS was constructed. Models were run with the same fluxes and without chemistry to isolate transport differences. Further, two COS flux scenarios were compared: one using a biosphere flux with a monthly time resolution and the other using a biosphere flux with a three-hourly time resolution. In addition, we investigated the sensitivity of the simulated concentrations to different biosphere fluxes and to indirect oceanic emissions through dimethylsulfide (DMS) and carbon disulfide (CS_2). The modelled COS mixing ratios were assessed against in-situ observations from surface stations and aircraft.

The results indicate that all models fail to capture the observed latitudinal distribution of COS at the surface. The COS mixing ratios are underestimated by at least 50 parts per trillion (ppt) in the tropics, pointing to a missing tropical source. In contrast, in summer the mixing ratios are overestimated by at least 50 ppt above 40°N, pointing to a likely missing sink in the high northern latitudes during the summer. The seasonal variability and the latitudinal distribution of COS surface mixing ratios are more sensitive to the transport model used than to a change in biosphere fluxes. Regarding the seasonal mean latitudinal profiles, in the vicinity of anthropogenic sources, the spread between models is greater than 60 ppt above 40°N in boreal summer. Regarding the seasonal amplitude, the model spread reaches 50 ppt at 6 out of 15 sites, compared to an observed seasonal amplitude of 100 ppt. All models simulated a too late minimum by at least 2 to 3 months at two high northern-latitude sites, likely owing to errors in the seasonal cycle in the ocean emissions. Finally, the temporal resolution of the biosphere fluxes (monthly versus three-hourly) has a relatively small impact of less than 20 ppt (compared to model spread) on the mean seasonal cycle at surface stations.

1 Introduction

Carbonyl sulfide (COS) is a rather long-lived sulphur-containing trace gas with a mean atmospheric mixing ratio less than 500 parts per trillion (ppt). Due to its long lifetime (~2.5 years), COS reaches the stratosphere, where its decay products contribute to the formation of Stratospheric Sulfur Aerosol (SSA). COS is emitted directly and indirectly by the ocean and industrial activities, directly by biomass burning and anoxic soils (Whelan et al., 2018). The main sink of COS is the uptake by the biosphere (Campbell et al., 2008; Blake et al., 2008; Suntharalingam, P. et al., 2008; Berry et al., 2013a), with minor sink contributions also from chemical break-down in the troposphere and stratosphere (Whelan et al., 2018). COS is taken up in leaves through similar pathways as carbon dioxide, but without significant respiration (Protoschill-Krebs et al., 1996;

Wohlfahrt et al., 2012). For this reason, COS has been proposed as a tracer that can be used to infer Gross Primary Productivity (GPP) at large scale.

To infer GPP from COS, we need several pieces of information that are currently still highly uncertain. First and for all, the current flux estimates do not lead to a closed COS budget that is in line with the near-constant COS burden in the atmosphere from 2000 up to 2015 (Whelan et al., 2018). Several studies suggest that sources are missing from the tropical oceans (Berry et al., 2013a; Kuai et al., 2015; Glatthor et al., 2015; Launois et al., 2015b; Remaud et al., 2022), but currently no hard evidence has been obtained from shipboard measurements (Lennartz et al., 2017; Lennartz et al., 2020b; Lennartz et al., 2021a). Recent inverse modelling studies (Ma et al., 2021, Remaud et al., 2022) confirm the need for a tropical source of COS (or a reduced tropical sink) and more COS uptake at high Northern latitudes. Interestingly, while the results of Ma et al. (2021) point to too low modelled COS mixing ratios in the free troposphere, Remaud et al. (2022) could not confirm this finding. This discrepancy triggers the question how well atmospheric transport models are able to simulate the global COS distribution. Since the source-sink distribution of COS is distinctly different from that of CO2, a COS model comparison may lead to additional information relative to earlier comparisons that were conducted within the atmospheric tracer transport model intercomparison project TransCom (Law et al., 1996; Gurney et al., 2002). For instance, the one-way uptake of COS by the biosphere both during day and night (Kooijmans et al., 2021; Maignan et al., 2021) differs from the CO2 interaction with the biosphere with respiration at night and uptake dominating during daytime. On larger scales, the seasonal cycle of COS shows strong signs of biosphere uptake in the Northern Hemisphere (NH) summer and ocean emissions in the Southern Hemisphere (SH) (Montzka et al., 2007). As a result, the gradient between the NH and SH changes seasonally, and in a different way than the CO2 gradient.

It is however important to realise that the various terms in the COS budget are currently still very uncertain. It is therefore important to study the behaviour of various surface flux terms in a variety of models, to investigate whether different models point to similar inconsistencies in the global COS budget. The aim of this paper (and a complementary paper, part 2) is to analyse results from a model intercomparison study that focuses on COS. Specifically, we address the questions:

1 - What are the comparative roles of uncertainties in transport versus emission distribution in simulating the interhemispheric (IH) gradient, seasonal cycle and vertical profiles of COS?

2- How large is the model-to-model spread compared to the mismatch between model and observations (i.e. how sure are we that there is something wrong with the fluxes?)

3 - What is the sensitivity of simulated tropospheric COS mixing ratios to the diurnal variability in COS biosphere fluxes?

The latter question has been addressed before in TransCom for CO2 simulations, and is commonly referred to as a (diurnal) rectifier effect (Denning et al., 1995; Denning et al., 1999). Simply said, the question addresses the issue whether the use of monthly mean biosphere fluxes is sufficient to reliably simulate the COS tropospheric seasonal cycle, or should the biosphere be resolved on higher time resolution?

To answer these questions the paper is structured as follows: Section 2 describes the modelling protocol, the participating models, and the measurements that were used to evaluate the models, Section 3 presents the results, and Section 4 ends with a discussion and conclusions. While Part one of this study focuses on model simulations with prescribed bottom-up fluxes, Part two focuses on the two sets of fluxes that were optimized using atmospheric surface observations.

2 Participating models and outputs

2.1 Participating models and outputs

Seven atmospheric transport models participated in the inter-comparison of modelled COS mixing ratios. These models represent the diversity existing in the research community. The main features of each transport model, i.e. the horizontal and vertical resolution, meteorological drivers are given in Table 1. Almost all models use meteorological fields from atmospheric reanalysis (ERA5, ERA-interim, NCEP, and JRA-55), either by direct use, or by nudging toward fields of horizontal winds (e.g LMDz; MIROC4). The TOMCAT Atmospheric Transport Model (ATM) is forced toward fields of surface pressure, vorticity, and divergence from ERA-Interim. For this model and for TM5, the convective mass fluxes are taken from ERA-Interim and interpolated to the model grid, which has a coarser resolution than ERA-Interim. In terms of resolution, NICAM6 has the highest horizontal resolution (~1°) while the TM3 ATM has the coarsest resolution (~5°x4°).

The vertical mixing in the convective boundary layer is represented with different parameterizations in the different models. For deep convective mixing, parameterizations rely on the mass-flux approach and are mainly adapted from three convective schemes: the Arakawa and Schubert (1974) scheme (MIROC4, NICAM 5&6), the Tiedtke (1989) scheme (TM3) and the Emmanuel et al. (1991) scheme (LMDz). The convective mass fluxes from ERA-Interim given to the TOMCAT and TM5 ATMs is based on a modified version of the Tiedtke (1989) scheme in the European Centre for Medium-Range Weather Forecasts (ECMWF)'s Integrated Forecasting System (Bechtold et al., 2014). The Arakawa and Schubert (1974) scheme spectrally represents multiple cloud types with different cloud base mass fluxes. The Tiedtke (1989) scheme is a single plume entraining-detraining model. The Emmanuel (1991) convective scheme, implemented in LMDz, represents an ensemble of cumulus by an undilute updraft and a spectrum of mixtures with the environmental air. The subgrid scale parameterization schemes are also referenced in Table 1, although most of them have been modified from their original formulations. In most of them, the sensitivity of the convective development to environmental humidity has been enhanced either by setting up a threshold based on relative humidity to prevent deep convection from triggering too often (MIROC4, Patra et al., 2018) or by increasing the entrainment of air from the environment in the mixtures (LMDz, Grandpeix et al., 2004) or in the plume (NICAM, Chikira and Sugiyama, 2010) when the environment is too dry. In LMDz, the convective triggering is now based on sub-cloud scale processes and not on the Convective Available Potential Energy (CAPE) anymore, improving the diurnal cycle of convection (Rio and Hourdin, 2008).

Transport model	Meteorology	Horizontal and vertical resolutions	Reference	Convection scheme	PBL mixing scheme	Advection scheme

LMDz	Nudging towards horizontal winds from ERA-5	1.875º×3.75º, 39η	Remaud et al. (2018)	Emanuel (1991); Rochetin et al. (2013)	Small scale turbulence: Mellor and Yamada (1974) Shallow convection: Rio and Hourdin. (2008)	Leer (1997); Hourdin and Armengaud (1999)
TM5	Meteo-and surface fields from ERA-Interim	2ºx2º, 25η	Krol et al. (2005)	Convective mass fluxes from ERA-Interim	Near surface mixing: Louis (1979); Free troposphere mixing: Holtslag and Moeng (1991)	Slopes advection scheme: Russell and Lerner (1981)
TM3	Meteo-and surface fields from NCEP	4ºx5º, 19η	Heimann et al., 2003	Tiedtke (1989)	Louis (1979)	Slopes advection scheme: Russell and Lerner (1981)
TOMCAT	Forced with the surface pressure, vorticity, divergence from ERA-Interim	2.8º × 2.8º, 60η (surface to ~60 km)	Chipperfield (2006)	Convective mass fluxes from ERA-Interim	Louis (1979)	Prather (1986)
MIROC4	Nudging towards horizontal winds and temperature from JRA-55	T42 spectral truncation (~ 2.8º × 2.8º), 67η	Patra et al. (2018)	Arakawa and Schubert (1974), with updates	Mellor and Yamada (1982)	Lin and Rood (1996)
NICAM5	Nudging towards horizontal	~223 km (icosahedral grid), 40z*	Niwa et al. (2017)	Chikira and Sugiyama (2010)	MYNN (Mellor and Yamada, 1974;	Miura (2007) & Niwa et al. (2011)

	winds from JRA-55				Nakanishi and Niino, 2004) Level 2 scheme	
NICAM6	Nudging towards horizontal winds from JRA-55	~112 km (icosahedral grid), 40z*	Niwa et al. (2017)	Chikira and Sugiyama (2010)	MYNN (Mellor and Yamada, 1974; Nakanishi and Nino, 2004) Level 2 scheme	Miura (2007) & Niwa et al. (2011)

Table 1: Main characteristics (vertical resolution, horizontal resolution, meteorological drivers, transport and sub-grid parameterization schemes) of the TransCom models used in this experiment. η vertical coordinates are a hybrid sigma-pressure coordinate and z* is the terrain-following vertical coordinate based on the geometric height.

Simulations were performed using meteorology and surface emissions for the period from 2010 to 2018. The two first years are considered as spin-ups and therefore not included in the analysis. As this study focuses on the spatio-temporal COS variability and the COS budget is currently not closed (see Table 3), we do not attempt to reproduce the observed mean COS values and the simulations started from a null initial state. For simplicity, oxidation within the troposphere, estimated as 100 GgS.yr−1, photolysis in the stratosphere, estimated as 35-60 GgS.yr−1, have not been considered, enabling to isolate the influence of transport processes on COS tropospheric variability.

Model output was generated at each measurement time and location used in the analysis as an hourly average. Modelers chose the horizontal positions to report simulated concentrations; either from a nearest grid point value, or interpolated to the site location from values at surrounding grid points. Additionally, 3-D fields of monthly mean COS mixing ratios were stored and analyzed. Higher temporal resolutions were not considered since this study only looks at seasonal and longer timescales, and to prevent excessively large file sizes. A more complete description of each ATM is given in Annex A.

2.2 Prescribed flux components

The prescribed COS flux components used as model inputs are presented in Table 2. Each participating group interpolated the emissions horizontally in space to their (coarser) model grid, while ensuring mass conservation. Subsequently, the fluxes provided lower boundary conditions of each atmospheric transport model, which then simulates the transport of COS by the atmospheric flow. Relying on the linearity of the atmospheric transport, each flux of each scenario was transported separately by all participating models, and the various concentration contributions of the individual fluxes were then added for different scenarios (i.e. combination of fluxes) as described in section 2.4.

191

Process	**Name**	**Time resolution**	**Spatial resolution**	**Period**	**Reference**	**Total global flux (GgS.yr−1)**
Vegetation + soil from SIB4	BIO_SIB4	monthly, interannual	1° x 1°	2010-2018: monthly fluxes	Kooijmans et al., 2021	-669 (vegetation) -91 (soil)
Vegetation + soil from SIB4	BIO_SIB4_Diurnal	3-hourly	1° x 1°	2015: 3-hourly fluxes	Kooijmans et al., 2021	-654 (vegetation) -92 (soil)
Vegetation + soil from ORCHIDEE	BIO_ORC	monthly, interannual, 3-hourly	0.5 x 0.5°	2010-2018: monthly fluxes, 2015: 3-hourly fluxes	Maignan et al., 2021 Abadie et al., 2022	-531 (vegetation) -264 (soil)
Biomass burning	BB	monthly,interannual	1° x 1°	2010-2016	Stinecipher et al., 2019	+53
Anthropogenic	ANT	monthly, interannual	1° x 1°	2010-2015	Zumkehr et al., 2018	+397
Direct oceanic emissions + indirect emissions from CS_2	OCE	monthly, interannual	T42 grid (ca. 2.8x2.8°)	2010-2018	Lennartz et al., 2017; Lennartz et al., 2021	+203
Indirect oceanic emission via DMS	OCE_DMS	monthly, interannual	T42 grid (ca. 2.8x2.8°)	climatological	Lennartz et al., 2017; Lana et al., 2012	+70
Indirect oceanic emissions via DMS from NEMO PISCES	OCE_DMS_PISCES	monthly,climatological	91x144 (2°x2.5°)	climatological	Belviso et al., 2012	+119

Table 2: Prescribed COS surface fluxes used as model input. Mean magnitudes of the fluxes are given in $GgS.yr^{-1}$ for the period 2010–2018.

The biosphere fluxes BIO_SIB4 and BIO_ORC, simulated by the SIB4 Land Surface Model (LSM) (Kooijmans et al., 2021) and the ORCHIDEE LSM (Maignan et al., 2021, Abadie et al., 2022), respectively, include the COS absorption by vegetation and the oxic soil fluxes. In both LSMs, the absorption by plants is parameterized following the Berry et al. (2013) model, which was rescaled with varying COS surface mixing ratios and slightly adapted to represent the COS absorption at night that arises from incomplete stomatal closure (Kooijmans, et al., 2021, Maignan et al., 2021). The spatially varying COS mixing ratios are from a monthly climatology that was obtained by transporting the optimized COS fluxes by Ma et al. (2021) with the TM5 ATM. The soil fluxes include the COS irreversible uptake via hydrolysis parameterized with the Ogee et al. (2016) model and an abiotic production term. In the ORCHIDEE LSM, the abiotic term is parameterized following the approach described in Whelan et al. (2016) while, in the SIB4 LSM, it is based on Meredith et al. (2018). The emissions from anoxic soils are not considered in this study because of the absence of reliable emission estimates at the beginning of this study.

The direct oceanic emissions of COS (including indirect emissions from CS2) are derived from a box model approach (Lennartz et al., 2021). The indirect oceanic emissions of COS through DMS, OCE_DMS_PISCES and OCE_DMS, are based on two different approaches. OCE_DMS is a monthly climatology produced from extrapolations of measurements in sea waters distributed unevenly around the globe (Lana et al., 2011). OCE_DMS_PISCES is simulated by a mechanistic model of DMS production implemented in the Ocean General Circulation Model NEMO-PISCES (Belviso et al., 2012). It should be noted that the climatology of Lana et al., 2011 has been recently updated using additional sea water measurements and a refined extrapolation method (Hulswar et al., 2022). The spatial distribution of the new DMS fluxes is now closer to the mechanistic representation of these fluxes from Belviso et al. (2012) with larger summer emissions in the southern high latitudes.

The open burning inventory emissions from Stinecipher et al. (2019), available for the period 1997–2016, include emissions from savanna and grassland, boreal forests, temperate forests, tropical deforestation and degradation, peatland fires, and agricultural waste burning. The inventory is obtained from CO emissions using the GFED Global Fire Emissions Database (GFED version 4, https://www.globalfiredata.org/). Biomass burning sources from agricultural residues and biofuels were not included in the absence of a global map although they were shown to be 3 times as large as open burning emissions over northern America (Campbell et al., 2015). In the Supplement, the Stinecipher et al. (2019) inventory is compared with the GFED v4.1 and Community Emissions Data System (CEDS) (Hoesly et al., 2018) (see Fig. S11), that includes additional biofuel use, with a global total of 118–154 $GgS.yr^{-1}$ over the period 2010-2018 estimated in Ma et al. (2021). Choosing one inventory over the other is not expected to change the findings of this study.

The Zumkher et al., 2018 inventory includes, in order of importance, anthropogenic emissions from the rayon (staple and yarn) industry, residential coal, pigments, aluminum melting, agricultural chemicals, and tyres. These emissions arise both from direct COS emissions and indirect COS emissions through atmospheric oxidation of CS_2, that is supposed to be instantaneous and to occur at the surface. The anthropogenic emissions are mainly located over China and Europe.

2.3 Measurements and data sampling

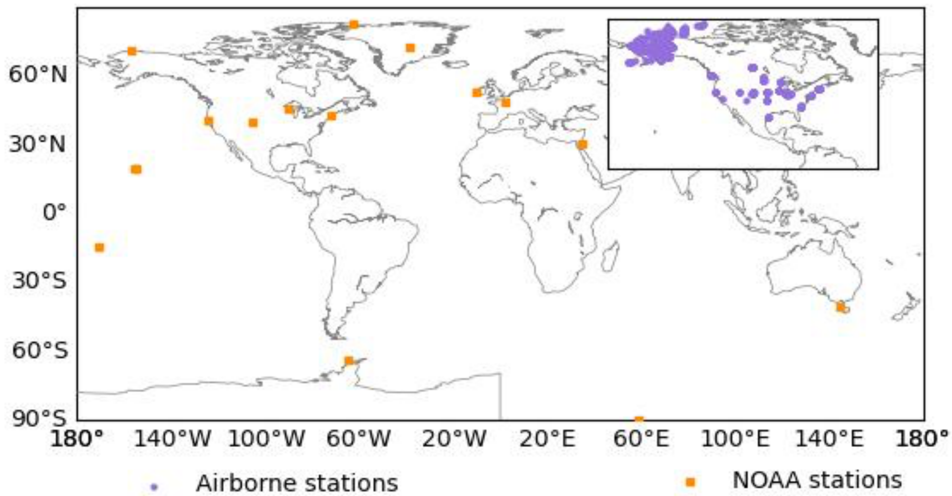

Figure 1. Geographical locations of the NOAA ground-based observations (orange squares) and the NOAA profile programme (inset).

We evaluated the simulations of COS mixing ratio against the NOAA/ESRL measurements between 2010 and 2018 at 15 sites: Cape Grim, Australia (CGO, 40.4°S, 144.6°W, 164 m above sea level, asl), American Samoa (SMO, 14.2°S, 170.6°W, 77 m asl), Mauna Loa, United States (MLO, 19.5°N, 155.6°W, 3397 m asl), Cape Kumukahi, United States (KUM, 19.5°N, 154.8°W, 3 m asl), Niwot Ridge, United States (NWR, 40.0°N, 105.54°W, 3475 m asl), Wisconsin, United States (LEF, 45.9°N, 90.3°W, 868 m asl—inlet is 396 m above ground on a tall tower), Harvard Forest, United States (HFM, 42.5°N, 72.2°W, 340 10 m asl, inlet is 29 m aboveground), Barrow (named also Utqiagvik), United States (BRW, 71.3°N, 155.6°W, 8 m asl), Alert, Canada (ALT, 82.5°N, 62.3°W, 195 m asl), Trinidad Head, United States (THD, 41.0°N, 124.1°W, 120 m asl), Mace Head, Ireland (MHD, 53.3°N, 9.9°W, 18 m asl), Weizmann Institute of Science at the Arava Institute, Ketura, Israel (WIS, 29.96°N, 35.06°E, 151 asl), Palmer Station, Antarctica, United States (PSA, 64.77°S, 64.05°W, 10.0 asl), South Pole, Antarctica, United States (SPO, 89.98°S, 24.8°W, 2810.0 asl) and since mid-2004 at Summit, Greenland (SUM, 72.6°N,38.4°W, 3200 m asl). The COS samples have been collected as paired flasks one to five times a month since 2000 and have been analysed with gas chromatography and mass spectrometry detection. Most measurements have been performed in the afternoon between 11 and 17h local time when the boundary layer is well mixed, thereby optimizing the comparability with model simulations. Only COS measurements with a difference between the paired flasks of less than 6.3 ppt are considered. These data are an extension of the measurements first published in Montzka et al., 2007. In addition, we used the French sampling site, GIF (48.7°N - 2.1°'E), located about 20 km to the south west of Paris where ground level COS has been monitored on an hourly basis since August 2014 (Belviso et al., 2022).

To investigate the impact of transport errors on the vertical distribution of COS, we compared model results to 2012–2016 NOAA airborne data located at 11 sites over North America. The upper altitude that was typically reached by this sampling program is 8 km.

2.4 Emission scenarios: the different experiments

The bottom-up emission scenarios with their associated source and sink components of COS considered in this study are described in Table 3. The control (**Ctl)** scenario represents the state of the art in the COS global budget, as it combines the main known COS fluxes. Only volcano emissions, in the range 23-43 GgS.yr^{-1}, and emissions from anoxic soils, have not been considered (Whelan et al., 2018). Compared to previous studies (see Table 1 of Remaud et al., 2022), the budget for **Ctl** is almost closed with an imbalance of only -37 GgS.yr−1 and leads to nearly stable atmospheric mixing ratios at surface sites (see Fig S1). However, we didn't take into account the chemical removal terms in this study: the photolysis loss of COS in the stratosphere amounting to around 50 GgS.yr−1 and the oxidation loss of COS in the troposphere amounting to around 100 GgS.yr−1 (Whelan et al., 2016). If the chemical removal terms were included, the budget would be negatively unbalanced by 200 GgS.yr−1, which deviates from the -37 GgS.yr−1.

The **Diurnal** scenario differs from the **Ctl** scenario in that it uses biosphere fluxes (soil and vegetation) with a 3-hourly temporal resolution instead of a monthly resolution. Comparing scenarios **Ctl** and **Diurnal** addresses research question 3.

The two last emission scenarios, **Bio2** and **Ocean2**, aim to investigate the influence of a change in terrestrial and oceanic fluxes on atmospheric surface mixing ratios. The **Bio2** scenario differs from the **Ctl** scenario in that the biosphere fluxes are provided by the ORCHIDEE LSM instead of the SIB4 LSM. The **Ocean2** scenario differs from the **Ctl** scenario in that the DMS oceanic fluxes are provided by the NEMO-PISCES ocean model instead of the climatology of Lennartz et al. (2017).

Name	Transported fluxes	Source-Sink Balance	ATMs
Ctl	ANT+BB+OCE+OCE_DMS+BIO_SIB4 (monthly)	-37 GgS.yr−1	All (see Table 1)
Diurnal	ANT+BB+OCE+OCE_DMS+BIO_SIB4_Diurnal	12 GgS.yr−1	LMDz, TM5, TM3, MIROC4, NICAM5, NICAM6
Bio 2	ANT+BB+OCE+OCE_DMS+BIO_ORC	-72 GgS.yr−1	LMDz
Ocean 2	ANT+BB+OCE+OCE_DMS_PISCES+BIO_ORC	11.7 GgS.yr−1	LMDz

Table 3: Description of the emission scenarios. Note that the budget does not include chemical removal terms of ~150 GgS.yr−1 (Whelan et al., 2018).

2.5 Post-processing of the simulations and measurements

In Sect. 3, the features of interest (annual mean, monthly smoothed seasonal cycle) are derived from the surface mixing ratios using the CCGVU curve fitting procedure developed by Thoning et al. (1989) (Carbon Cycle Group Earth System Research Laboratory (CCG/ESRL), NOAA, USA). The CCGVU procedure is fully described and freely available at http://www.esrl.noaa.gov/gmd/ccgg/mbl/crvfit/crvfit.html. The procedure estimates a smooth function by fitting the time series to a first-order polynomial equation for the growth rate combined with a two-harmonic function for the annual cycle and with the residuals that are filtered with a low-pass filter using 80 and 667 days as short-term and long-term cutoff values, respectively. The seasonal cycle and annual gradient are extracted from the smooth function. In addition, outliers are discarded if their values exceed 3 times the standard deviation of the residual time series.

3 Results

3.1 Impact of different transport models: using one flux scenario

3.1.1. General behavior: zonal mean structure

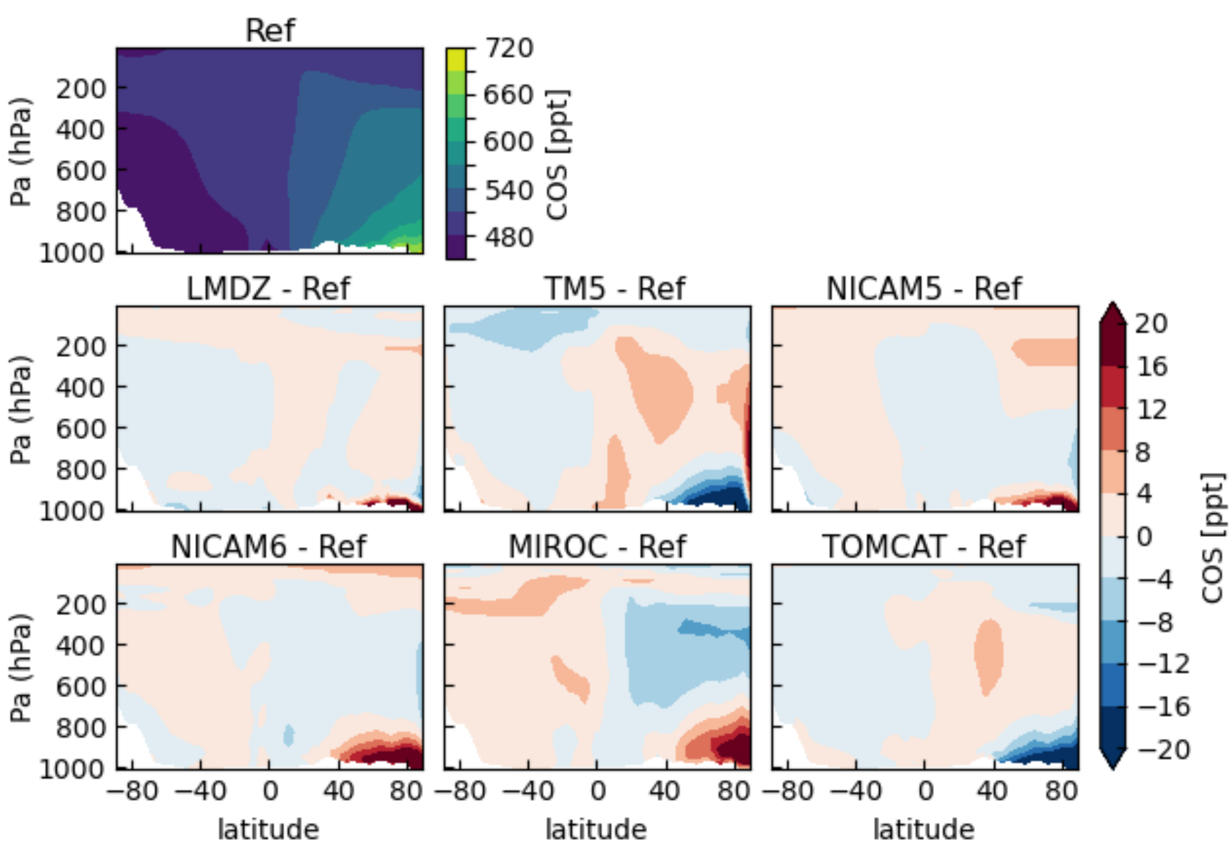

Figure 2. Zonal mean mole fraction of COS (ppt) for the reference for the **Ctl** scenario (top row). The reference is the average of COS over all transport models, calculated for the summer months (June, July, August) in 2012–2018. The resulting COS abundances have been shifted by +396 ppt, which brings the reference close to the observed concentrations averaged over all surface sites for January averaged over the years 2012-2018. Second and third rows: Zonal mean mole fraction difference between each individual transport model and the reference.

We first study the zonal mean structure of the COS simulations. We focus on the boreal summer (June-July-August - JJA) as convection is more active over the continents in the NH, which causes the spread among the models to be the largest. Moreover, the use of COS as a photosynthesis tracer requires quantifying the transport errors during boreal summer, when photosynthesis is more active.

With the **Ctl** scenario, Figure 2 shows that the zonal mean distribution of COS averaged over the transport models exhibits a strong meridional gradient in boreal summer with higher COS values in the NH. The COS source outweighs the terrestrial sink, leading to a net accumulation of COS mole fractions at the surface during winter. The reader is referred to Section 3.2 for a decomposition of the COS total surface mole fractions into the signals caused by the different COS budget components. In addition, Figure 2 depicts the zonal mean distribution of the difference of COS mole fractions between each model and the multi-model average. The effect of the transport differences is the largest below 800 hPa and exceeds 50 ppt above 40°N, where surface fluxes are the largest. The spread of COS mole fractions at the surface reflects different strengths of vertical mixing within the tropospheric column. Indeed, a positive anomaly of surface COS mole fractions at the surface compared to the multi-model average is often associated with a negative anomaly in the mid-troposphere. In particular, higher surface mole fractions of COS in the NICAM, MIROC4 and LMDz ATMs suggests that there is, on average, less convection penetrating into the upper troposphere in these models compared to the TM5 and TOMCAT ATMs. The comparison between the NICAM5 and NICAM6 ATMs indicates a modest contribution of the model horizontal resolution to the model spread, as observed by Lin et al. (2018). This is also in agreement with Remaud et al. (2018) who showed that the convective and the planetary boundary layer parameterization schemes have larger impact on the CO_2 mole fractions in the low and mid troposphere relative to the impact of horizontal and vertical resolutions.

In the three models exhibiting less vertical mixing, two of them, the TOMCAT and TM5 ATMs use the convective masses fluxes from the ERA-Interim reanalysis extrapolated to their lower resolution model grid. The TM3 ATM is based on the Tiedtke et al. (1989) which has been recognized to trigger convection too often (Hirons et al., 2013). In the models exhibiting less vertical mixing, the original formulation of the convective schemes has been modified to depart from the convective quasi-equilibrium assumption proposed by Arakawa and Schubert (1974) and to prevent deep convective clouds from developing too often, especially in a too dry environment. In the LMDz ATM, the original closure based on the CAPE of the Emanuel (1991) scheme was replaced by a closure based on sub-cloud processes that enables deep convection to be delayed later in the afternoon and reduced in intensity (Rio and Hourdin, 2008). The entrainment function in the mixtures has also been modified to be more sensitive to relative humidity of the environment (Grandpeix et al., 2004). In the MIROC4 ATM, a threshold as a function of relative humidity has been implemented in the Arakawa and Schubert (1974) scheme to prevent convection from triggering when the relative humidity is too low. In the NICAM ATM, the Chikira and Sugiyama (2010) scheme models the entrainment rate to vary vertically, depending on the humidity and temperature profiles. These implementations generally lead to a more realistic tropical variability (Lin et al., 2006) and could explain why the vertical mixing is weaker in MIROC 4, LMDz and NICAM.

It should be noted that, in consistency with previous studies (Patra et al., 2011a, Saito et al., 2013), the meridional gradient of COS reflects the intensity of the inter-hemispheric exchanges and seems to be controlled by the vertical gradient in the northern hemisphere. Indeed, in the middle troposphere, a negative anomaly of COS mixing ratio in the northern hemisphere is combined with a positive anomaly of COS mixing ratio in the southern hemisphere in most models exhibiting less vertical mixing (MIROC, NICAM 5 and 6). On the contrary, in models exhibiting stronger vertical mixing, a positive anomaly of COS in the northern hemisphere is associated with a negative anomaly of COS in the southern hemisphere.

3.1.2. Latitudinal gradient at surface stations

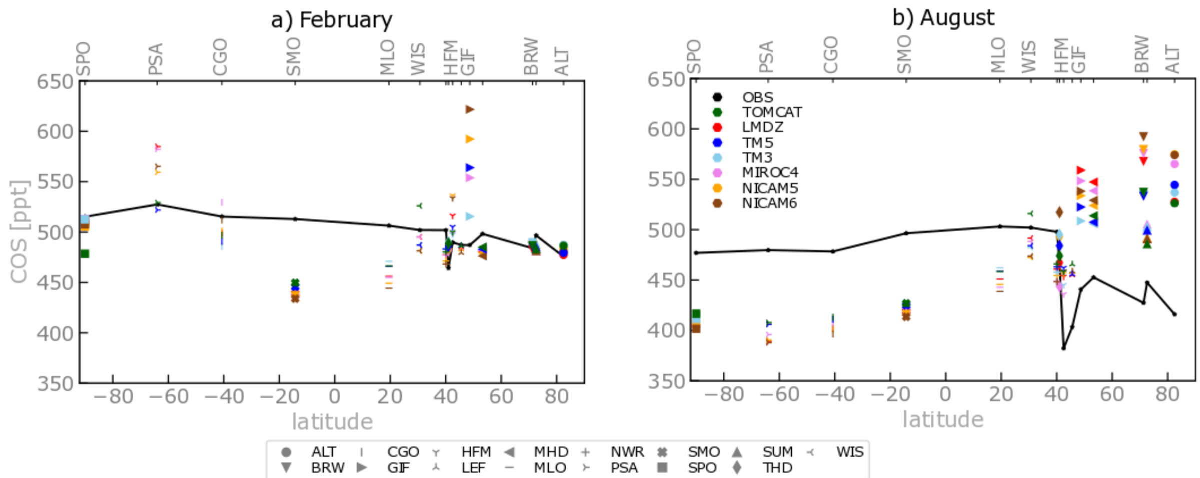

Figure 3: Comparison of the latitudinal variations of the COS abundance simulated by several transport models using the **Ctl** surface flux dataset (colored dots) with the observations (black line) for February (left), August (right) over the years 2012-2018. The simulated COS abundances have been shifted such that the means are the same as the mean of the observations (~500 ppt). The time series of COS mixing ratio have been detrended and filtered to remove the synoptic variability beforehand. In August, the value at site GIF simulated by the TOMCAT ATM was removed as it was an outlier (value above 800 ppt). For the same reason, the COS values at site GIF simulated by TOMCAT (800 ppt) and LMDz (around 700 ppt) have been removed in February. We removed the site KUM, which is co-located in longitude and latitude with site MLO, for the sake of simplicity.

The latitudinal gradient of COS mole fractions reflects the latitudinal surface flux distribution and the intensity of the interhemispheric exchange (Denning et al., 1999). Figure 3 shows the observed and simulated mixing ratios at the surface stations as a function of the latitude in February and August. The simulated COS mixing ratios are averaged over time at each surface station. Since the simulations start from a null initial state, the simulated COS mole fractions have been shifted by 500 ppt to match the annual mean COS observations. In February, the distribution of the observed surface mixing ratios is relatively flat over all latitudes. In contrast, all models exhibit a COS mole fraction which is 50 ppt lower in the tropics than elsewhere. This suggests that all the models agree on a missing source or a too strong biosphere sink over the tropics. Given the oceanic footprint of the tropical sites MLO and SMO, previous top-down studies of Remaud et al. (2022), Ma et al. (2021), and Berry et al. (2013) increased the oceanic source over the tropics to decrease the model-observation mismatch. The ATMs are unable to represent the negative gradient of 15 ppt from MHD to GIF (see also Fig. 11 of Remaud et al., 2022) and instead overestimate the mixing ratio at site GIF by up to 300 ppt. GIF is located in the vicinity of a misplaced hotspot of anthropogenic emissions in the Zumkher inventory (Remaud et al., 2022; Belviso et al., 2020) while in reality, GIF is comparable to a background station relatively far from major anthropogenic sources (Belviso et al., 2020). Overall, the model spread does not exceed 50 ppt at all sites except at sites PSA and GIF. The spread at PSA arises from a combination of strong oceanic emissions in austral summer and variation in vertical mixing. The spread at GIF is caused both by the ATM resolutions and the sub-grid scale parameterizations. Indeed, the ATMs with the highest vertical resolution, TOMCAT, NICAM 6 simulate mole fractions up to 300 ppt higher than the ATM with the lowest resolution, the TM3 ATM. It is well known that, as the model resolution increases, the simulated mixing ratios become more sensitive to the detailed distribution of sources that are defined with finer resolution. Likewise, the sensitivity to model errors is enhanced near emission hotspots. Errors in horizontal winds or errors in the vertical mixing can have a large impact with emissions from hotspots being nearby atmospheric stations, possibly creating biases. For instance, errors in horizontal winds can produce peaks which are not present in the observations (Locatelli et al., 2015a). Therefore, extra care should be taken when assimilating stations like GIF to optimize the COS surface fluxes in an atmospheric inverse framework (Remaud et al., 2022).

In August, the observed latitudinal distribution of COS was poorly captured by the ATMs. The observations exhibit a negative latitudinal gradient of almost 100 ppt between ALT and SPO. The lowest values of COS are located in the mid and high northern latitudes where the biosphere absorbs a substantial amount of COS from the atmosphere (Vesala et al., 2022, Maignan et al., 2021, Koojmans et al., 2021). In contrast, all ATMs simulate a positive interhemispheric gradient of 150 ppt between the northern and southern mid latitudes, with the highest values in the northern high latitudes. Overall, the deviation among models is much broader in August than in February, with a model spread exceeding 70 ppt in the northern high latitudes, for instance at BRW. This is due to the different intensities of the vertical mixing within the column (see Figure 1). The model spread does not exceed 15 ppt elsewhere but remains larger, by comparison, to the measurement uncertainty of 6 ppt.

3.1.3. Mean seasonal cycle at surface stations

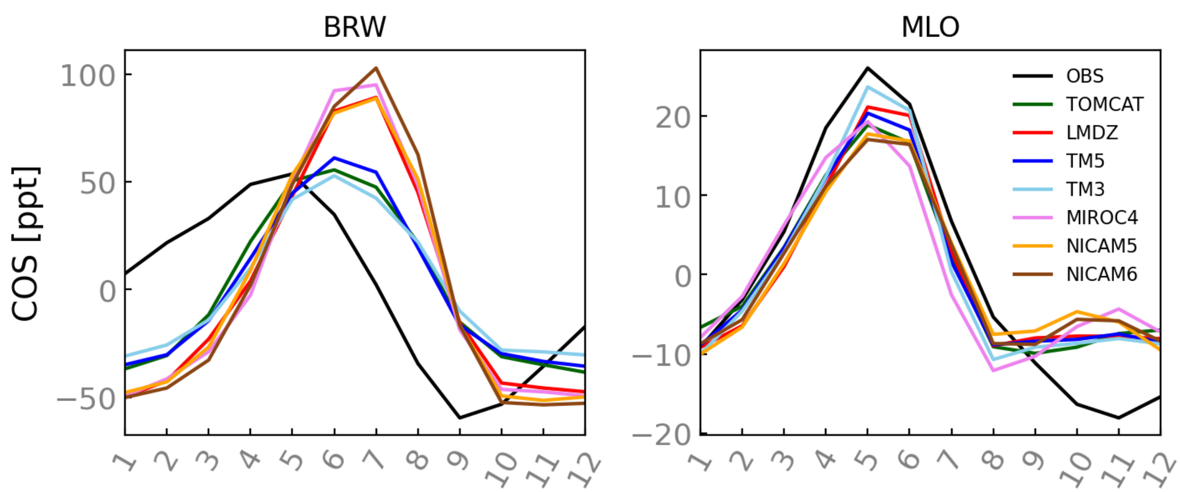

Figure 4 : Mean seasonal cycle of the observed (black) and simulated (color) COS mixing ratios at sites BRW and MLO. The curves have been detrended and filtered to remove the synoptic variability.

The impact of transport variability on the seasonal cycle is illustrated in Figure 4, which shows the mean seasonal cycle of COS given by all ATMs at sites BRW and MLO. BRW is a boreal station that samples mainly continental air masses coming from the mid and high latitudes (Parazoo et al., 2011). MLO is a background station with a strong maritime influence that samples air masses coming from the whole NH. Therefore, the seasonal amplitude at site BRW is twice as large as the seasonal cycle amplitude at site MLO. At site BRW, the simulated seasonal cycles lag that of the observations by 1 to 2 months in all transport models. In the observations, the mole fractions peak in May, whereas the modeled mole fractions peak in July. Focusing on the model spread, two groups of models can be distinguished: models with a large seasonal amplitude of 150 ppt and a weak vertical mixing (LMDz, NICAM5 & 6, MIROC4) and models with a small seasonal amplitude of 90 ppt and a strong vertical mixing (TOMCAT, TM3, TM5). It should be noted that the models with a large seasonal cycle amplitude have a steeper latitudinal gradient in August, as explained by Denning (1995). Compared to the site BRW, the models capture the phase of the seasonal cycle at site MLO relatively well, and their seasonal amplitudes diverge by not more than 20 ppt. However, all models underestimate the seasonal amplitude by 20 ppt and do not represent the observed minimum in November.

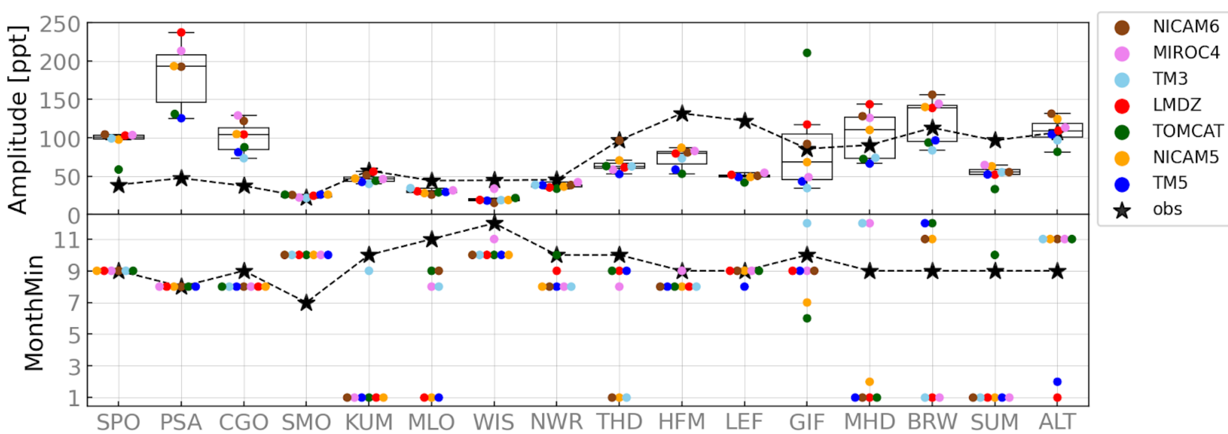

Figure 5: Top: Mean seasonal amplitude (maximum minus minimum mole fraction) of the observed (black stars) and simulated (colored dots) COS mole fraction at 15 surface sites. Each color dot corresponds to the mean seasonal amplitude of COS mixing ratio simulated by a different atmospheric transport model for the **Ctl** scenario. Boxplots of the mean seasonal amplitude of simulated COS mole fractions are superimposed. Bottom: Month of the minimum of the mean seasonal cycle for the observations (black) and for the several transport models (color dots). For each site, the COS time series have been detrended and filtered to remove the synoptic variability.

The performance of the transport models for the seasonal cycle amplitude is statistically evaluated for each surface station in the top panel of Figure 5. The complete mean seasonal cycle for each station and each model is shown on Figure S4 in the Supplement. The models capture the seasonal cycle amplitude well at the low latitude sites SMO, KUM, MLO, WIS, and at site NWR. These sites, representative of background air masses, exhibit a small seasonal amplitude of less than 50 ppt. At the most southern sites (SPO, PSA, CGO), the models overestimate the seasonal amplitude by at least 50 ppt. Since these stations sample air masses mainly coming from the Southern Ocean

(Remaud et al., 2022, Montzka 2007), an overestimated amplitude is likely caused by too strong oceanic emissions in summer. In contrast, the seasonal amplitude is underestimated by 50 ppt at continental sites THD, HFM, and LEF. Since the seasonal amplitude to a great extent reflects the amount of COS absorbed by plants at these sites (Campbell 2008, Blake et al., 2008), a too small simulated seasonal cycle amplitude likely arises from a too weak photosynthesis sink during the growing season. Focusing on the transport errors, the spread is greater than 50 ppt at site PSA, located in the Southern Ocean, and sites MHD, GIF, BRW, ALT. As illustrated in Figure 4, differences in the strength of the vertical mixing within the column mainly contribute to the model spread. Only at station GIF the resolution is also crucial. It should be noted that the mean mole fractions showed the largest model spread also at these stations. To evaluate the simulated seasonal cycle phase, the bottom panel of Figure 5 focuses on the month of the minimum concentration of the mean seasonal cycle for each site. A striking feature is that, at mid and high latitudes sites MHD, SUM, BRW, ALT, the seasonal minimum occurs in September in the observations. In the models, this minimum occurs up to 6 months later between October and January, as illustrated in Figure 4. At sites LEF, NWR, THD, HFM over Northern America, the models tend to simulate an earlier minimum crossing of at least one month. This might be related to the too weak terrestrial sink.

3.1.3. Mid-troposphere seasonal variations over Northern America

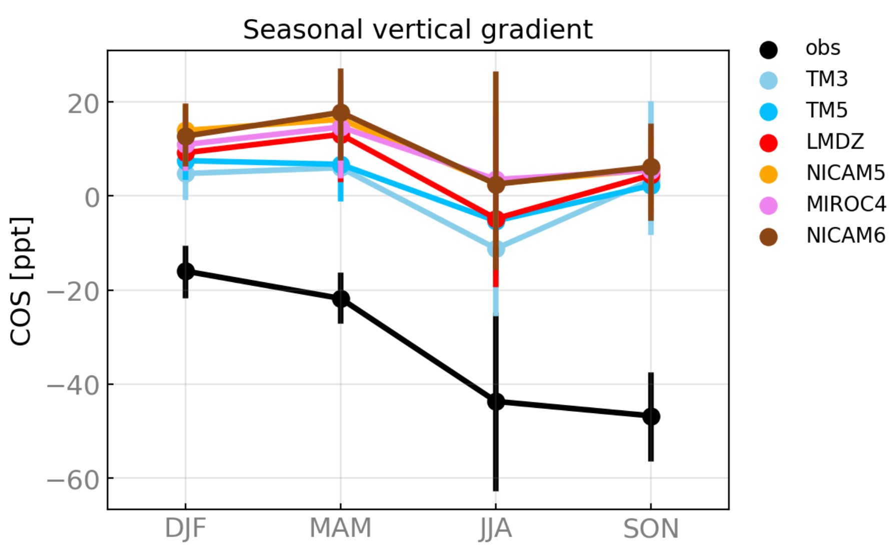

Figure 6. Seasonal mean observed and simulated COS gradient between 1 and 4 km (mole fractions at 1 km minus mole fractions at 4 km) averaged over airborne stations located over northern America for the **Ctl** scenario. For each subregion, the monthly COS gradients are calculated by averaging the differences in COS concentrations between 1 and 4 km over all the vertical profiles. For each season, the error bar represents the standard deviation of the seasonal COS gradient.

The vertical gradient between the boundary layer and the free troposphere reflects the effects of the surface fluxes and the atmospheric transport. Figure 6 shows the seasonal cycle of the vertical gradient of COS between altitudes of 1 km and 4 km averaged over the airborne sampling over Northern America (see Fig. 1). Since westerly winds prevail throughout the year in the entire free-troposphere at each site (Sweeney et al., 2015), oceanic air masses from the Pacific Ocean move across the North American continent and mix with air that has been in contact with the biosphere and anthropogenic emissions. Thus, these sites sample both continental and oceanic air masses, with the proportion of oceanic air decreasing from the West to the East of America. The observations show a negative mean vertical gradient throughout the year, decreasing from -20 ppt in DJF (December, January, February) to -50 ppt in SON (September to November). This suggests that, on average, continental Northern America behaves as a COS sink. The strongest decrease of 20 ppt occurs during the growing season in JJA. The large depletion of COS within the boundary layer seen in airborne profiles over Northern America has been reported previously to be concomitant to depletion of CO_2, indicating a strong and common biosphere sink during this season (Blake et al.,2008, Campbell et al., 2008, Parazoo et al., 2021).

Contrary to the observations, all ATMs show a mean positive vertical gradient all year round, except during JJA when gradients simulated by LMDz, TM3, and TM5 become slightly negative. The model spread is less than 10 ppt and reaches 15 ppt in JJA, much smaller than the mean bias of at least 30 ppt. The model spread and the observed and simulated standard deviation are higher in JJA. In summer, the weakening of the winds over the middle of the continent and over the east coast leads to less homogeneous vertical profiles in the free troposphere (Sweeney et al., 2015). Combined with enhanced convection, this effect might reinforce the model spread and the simulated standard deviation. Considering the model spread, the models underestimate the sharp decrease of vertical gradient in JJA by 50 % and do not prolong this decrease in SON. This model-observation mismatch is consistent with an underestimation of the mean seasonal cycle amplitude at sites HFM, LEF, THD. Kooijmans et al. (2021) showed that, on average, the SIB4 LSM using the Berry et al. (2013a) model for the plant uptake, combined to the Ogee et al. (2016) soil model with variable COS mole fractions, underestimates the COS terrestrial sink (soil and plant uptake) during the growing season over FLUXNET sites located in Europe and Northern America. Parazoo et al. (2021) came to the same conclusion by evaluating the SIB4 plant uptake against airborne measurements over three diverse regions in North America: the crop-dominated Midwest, evergreen-dominated South, and deciduous broadleaf-dominated Northeast. Photosynthesis was shown to peak later in the season over the humid temperate forest in the South compared to the SIB4 LSM (Parazoo et al., 2021), which is consistent here with an underestimated COS depletion in SON in Figure 5.

3.2 Impact of each flux components on COS surface mole fractions

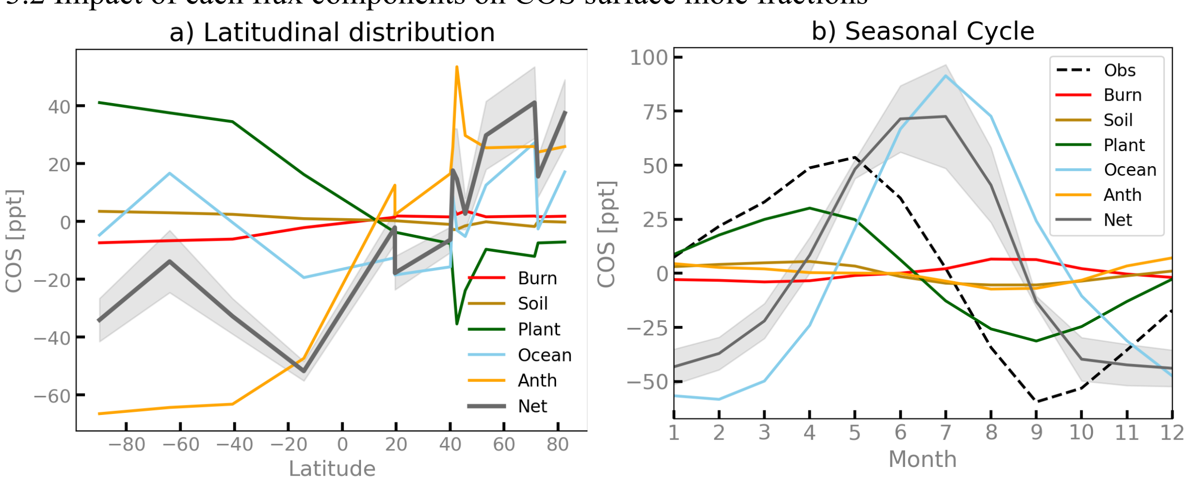

Figure 7: a) Simulations of the interhemispheric gradient of tropospheric COS mole fractions at NOAA surface stations. The net signal (gray line) is obtained from a multi-model average of global simulations using the **Ctl** emissions, while the colored lines are obtained by running the global atmospheric simulations with one component flux at a time. The shaded area represents the model spread. b) Simulations of the seasonal cycle of tropospheric COS mixing ratios at the Barrow Atmospheric Baseline Observatory (BRW) averaged over all transport models. The shaded area is the standard deviation around the mean COS seasonal cycle associated with the different transport models. The dotted black line represents the observed seasonal cycle.

In order to interpret the model-observation comparison of figure 3, Figure 7a presents the contributions of the COS budget components to the simulated interhemispheric gradient. Results represent the average over all ATMs participating in this intercomparison experiment. The strongly positive latitudinal gradient is driven by the anthropogenic component and to a lesser extent by the ocean emissions. The oceanic component is characterized by two mole fraction peaks in the Southern and Northern high latitudes and a minimum mole fraction in the tropics. The positive mole fractions at high latitudes result from the direct oceanic emissions in summer (Lennartz et al., 2017), the indirect emissions through DMS and CS_2 peaking in the tropics (Lennartz et al., 2021, see also Figure 2. of Remaud et al., 2022). On an annual basis, the plant uptake is characterized by a larger sink in the NH than in the SH. The resulting latitudinal gradient is however not sufficient to compensate for the opposing gradients from the ocean and anthropogenic emissions, leading to the overall mismatch observed in figure 3. The soil and the biomass burning components have a relatively flat distribution and therefore play a minor role in the latitudinal COS gradients.

Figure 7b shows the contributions of the COS budget components - oxic soils, ocean, plant uptake, anthropogenic emissions, biomass burning - to the detrended mean seasonal cycle at site BRW. The seasonality given by all ATMs is governed by the oceanic and plant uptake components. Since the anthropogenic fluxes do not vary throughout the year, the anthropogenic component of the simulated COS net concentrations is constant throughout the year, as expected. The weak seasonality of the soil component arises from the COS soil emissions in warmer conditions in summer that offsets the soil uptake in the Ogee et al. (2016) model that is implemented in the SIB4 model (See Fig 3. from Kooijmans et al., 2021). The one to two months lag between the observed and simulated concentrations at BRW (see figure 4) is thus likely induced by too strong oceanic direct emissions at high latitudes in summer or/and an underestimated plant sink in the boreal ecosystems of the NH. An enhanced plant uptake or/and reduced oceanic emissions in the summer high latitudes will also decrease the model observation-mismatch for the inter-hemispheric gradient (Figure 3). Using an atmospheric inverse framework, Remaud et al. (2022) found that an enhanced COS sink over the boreal regions associated with reduced oceanic summer emission in the Atlantic enables the simulated COS mole fractions to be in better agreement with the airborne measurements from the HIPPO campaign over the Pacific. From a bottom-up modeling perspective, there are some indications that the direct oceanic COS emissions could be overestimated and that the plant uptake is too low in boreal latitudes. For instance, the COS mole fractions given by the ocean box model are higher than most of the measurements made in sea waters sampled over different parts of the globe (Lennartz et al., 2017). In addition, Vesala et al. (2022) showed that the biosphere sink in LSMs was too small at a forested boreal site, Hyytiälä, in Finland. Scaled to all evergreen needleleaf forests over the whole boreal region, their empirical model calibrated on observations at Hyytiälä produces a biosphere COS sink that is consistent with the missing COS sink identified by our analysis.

3.3 Impact of different flux scenarios on COS surface concentrations: using the mean across transport models

3.3.1. Changing model fluxes

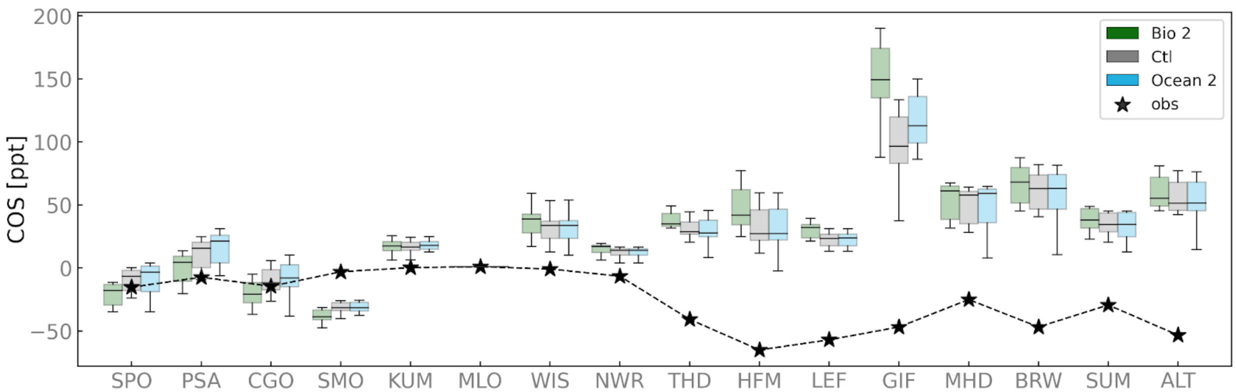

Figure 8: Box-plots of the simulated mole fraction gradient of COS between MLO and the other surface stations for the **Ctl** (gray), **Bio2** (green), **Ocean2** (blue) scenarios over the years 2012-2018 in August. The black stars denote the observed mean COS gradient between MLO and the other surface sites. The site codes are listed on the abscissa. For each site, the COS time series have been detrended and filtered to remove the synoptic variability.

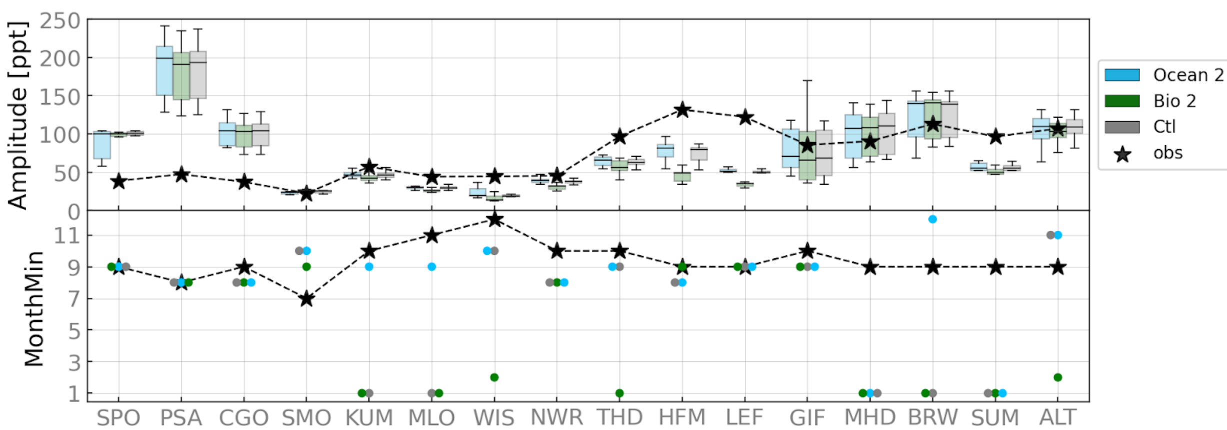

Figure 9: Top: Box-plots of the peak-to-peak amplitude (maximum minus minimum mole fraction) of the mean COS seasonal cycle for the **Ctl** (gray), **Bio2** (green), **Ocean2** (blue) scenarios over the years 2012-2018. The black stars correspond to the mean seasonal amplitude for the observed COS mole fractions. The sites are listed on the abscissa. Bottom: Mean time of minimum crossing for

modelled (colored dots) and observed (black stars) COS for each scenario. For each site, the COS time series have been detrended and filtered to remove the synoptic variability.

In this part, we assessed the sensitivity of the seasonal cycle and latitudinal distribution to a change in biosphere fluxes and indirect COS emissions through DMS oxidation. For the biosphere part, we consider two sets of biosphere fluxes produced by the ORCHIDEE LSM (**Bio 2** scenario) and the SIB4 LSM (**Ctl** scenario). Compared to the SIB4 LSM, land uptake in the ORCHIDEE LSM is 40 % lower over the tropical forests and over the eastern northern America (see Fig. S7). To assess the sensitivity of the COS surface mole fractions to a change in the ocean component, we compare the **Ctl** scenario against the **Ocean 2** scenario. The differences between the two fluxes is noticeable mainly over the subtropical oligotrophic gyres and over southern high-latitude oceans where the Belviso et al. (2012) DMS fluxes are 80% higher (see Fig. S8). In contrast, the latter are 50% weaker over the Western Pacific, which is not in line with the missing source location inferred by top-down studies (Remaud et al., 2022, Glatthor et al., 2015, Kuai et al., 2015). The updated version of the Lana et al. (2011) DMS climatology shows less DMS emissions over the Western Pacific and over the Southern Indian ocean (Hulswar et al., 2022). The reader is referred to Section 2.2 for a description of these oceanic and biosphere fluxes.

The annual gradient between a station and the MLO reference station relates to transport of source/sinks within the regional footprint area of the station as well as to the background gradient caused by remote sources. Figure 8 shows the boxplots of the mean annual gradients to MLO for all stations for the observations and all ATMs. As the stations are ranked according to their latitudes, Figure 8 enables us to compare the annual latitudinal repartition of COS simulated by all ATMs using three scenarios, **Ocean 2**, **Bio 2** and **Ctl**. Except at site GIF, the change in either biosphere fluxes or oceanic fluxes is translated into a change in mixing ratio that is smaller than 10 ppt and, also smaller than the model spread. The latter exceeds 50 ppt in the northern latitudes. At sites GIF, HFM, LEF, the annual gradient to MLO is more sensitive to the biosphere fluxes as the site is mainly influenced by continental air masses.

Figure 9 compares the mean seasonal cycle in terms of amplitude (top panel) and phase (bottom panel) simulated by all ATMs using three scenarios, **Ocean 2**, **Bio 2** and **Ctl**. On the amplitude, the effects of the biosphere and DMS fluxes are negligible compared to the model spread at most sites. The seasonal amplitudes at sites HFM and LEF are more sensitive to the biosphere fluxes than to the transport model and to the DMS fluxes as these sites sample continental air masses coming primarily from areas covered by vegetation. The site HFM is located in a forest that absorbs COS on average over the year (Commane et al., 2015). It should be noted that, at sites HFM and LEF, the ORCHIDEE LSM simulates smaller seasonal cycle amplitudes than the SIB4 LSM. This is first because the ORCHIDEE LSM has a smaller plant absorption of COS than the SIB4 LSM over northern America, also reflected by the global plant sink of COS (see Fig. S7) of -514 GgS.yr-1 (ORCHIDEE) versus -669 GgS.yr-1 (SiB4). Secondly, at site HFM (Harvard Forest), the soil fluxes of Abadie et al. (2022) have a smaller seasonal amplitude (Fig. 2 of Abadie et al. (2022)) than the soil fluxes from Kooijmans et al. (2021) (Fig. 3 of Kooijmans et al. (2021)). The absence of seasonal cycle in Abadie et al. (2022) is supported by the observations of soil fluxes at Harvard Forest. The too low seasonal cycle amplitude compared to the observations suggests again an underestimation of the COS plant uptake. Regarding the seasonal cycle phase on the bottom panel of Figure 9, the change of biospheric and oceanic fluxes has a minor effect (by one month) on the minimum crossing. Only the seasonal phases at sites KUM and MLO are affected by several months by the change of DMS fluxes as these two stations are located in the Pacific Ocean. Note however that the two biosphere models do not represent the current diversity of global LSMs which have much larger variation in photosynthetic fluxes (see for instance Annav et al., 2013) and the selected ocean variants only differ by the indirect oceanic emissions of COS through DMS (and not by the direct emissions).

3.3.2. Quantifying the diurnal rectifier effect on COS concentrations

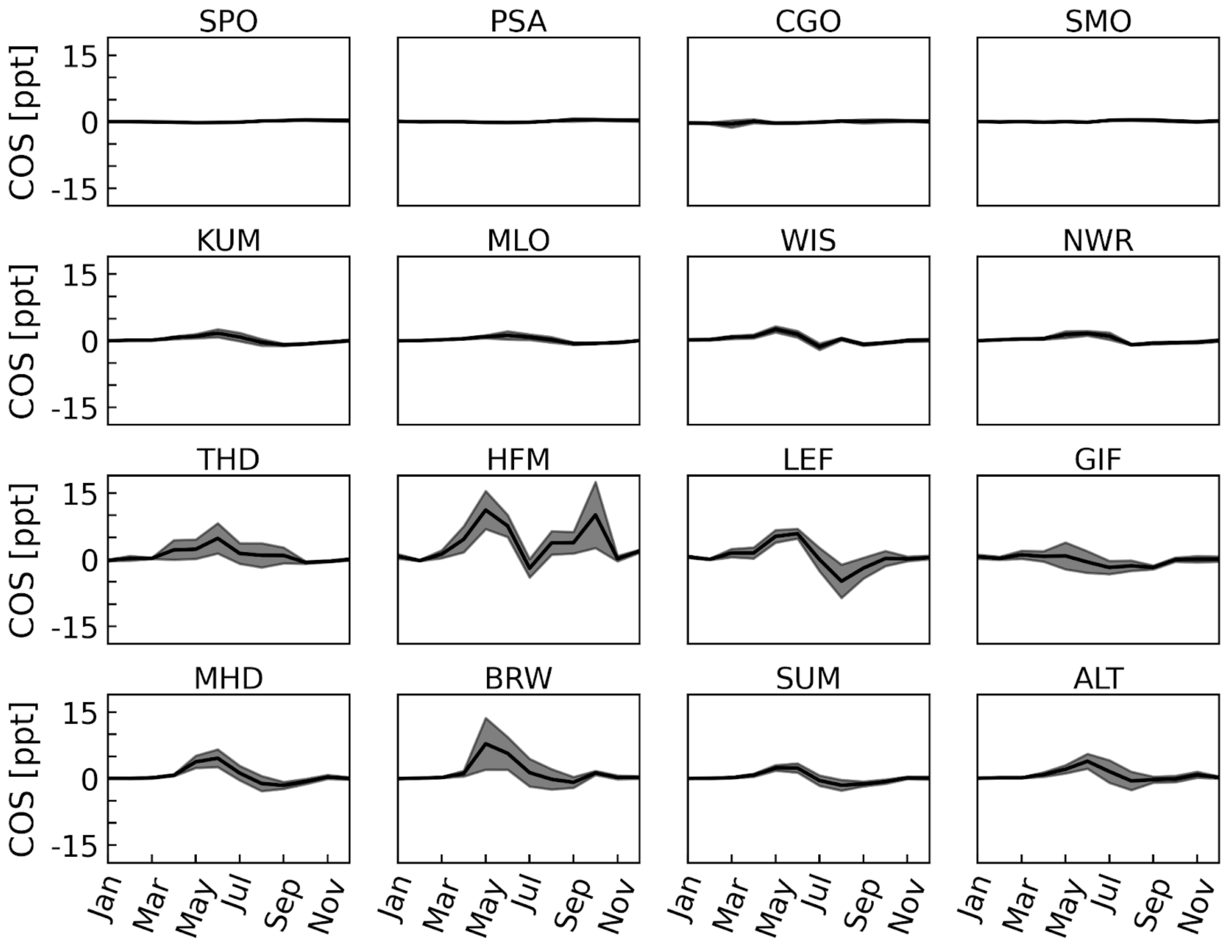

Figure 10: Monthly mean COS mole fractions obtained with the **Diurnal** scenario minus monthly mean COS mole fractions obtained with the **Ctl** scenario at each surface station for the year 2015. At each site, the solid line is the mean COS mole fraction across all models, and the shaded envelope represents the standard deviation around the mean.

The simulated COS diurnal variation reflects the day–night contrast in both the prescribed fluxes and the PBL (planetary boundary layer) vertical mixing. The diurnal variability comes here from the plant fluxes, with minor contribution from the soil fluxes. The plants absorb more COS during the daytime when the stomatal opening enables the photosynthesis to happen. At night, plants continue to absorb COS as the carbonic anhydrase activity does not depend on light intensity (Protoschill-Krebs et al., 1996; Goldan et al.,1998) and the stomatal closure is incomplete.

Observed nighttime uptake was shown to be on average 25 % of the daytime uptake across several sites located in Western Europe and Northern America between May–September (Kooijmans et al., 2021). Another part of the diurnal variability is contributed by boundary layer processes: during nighttime, COS accumulates near the surface within the shallower stable boundary layer, whereas during daytime, the low COS concentration caused by the plant uptake is distributed over a deeper convective PBL. Thus, the daily mean COS mixing ratio is expected to be greater than in the absence of boundary layer processes and diurnal plant variability (Denning et al. 1995; Dennin et al., 1999). This effect of the diurnal variability on longer time scales is called the diurnal rectifier effect.

We quantify here the diurnal rectifier effect on the seasonal variability of COS surface mixing ratios. To this end, Figure 10 shows the difference of monthly mean COS mixing ratio between the **Ctl** scenario and the **Diurnal** scenario for the year 2015 at 16 surface stations. In the **Ctl** scenario, the soil and plant fluxes are prescribed to the ATMs at monthly resolution whereas in the **Diurnal** scenario, the soil and plant fluxes are prescribed at a three-hourly resolution. Averaged over all ATMs, this effect is negligible and is less than the measurement uncertainties of 6 ppt at 11 stations out of 16. Even if the diurnal rectifier effect is more noticeable at sites HFM, LEF, BRW, the difference between the **Ctl** and **Diurnal** scenario does not exceed 20 ppt. In summer, the mainly positive difference in COS surface mixing ratios is induced by the temporal covariance between strong vertical mixing and stronger COS uptake during the day. The difference of monthly mean COS mixing ratio between the **Diurnal** scenario and the **Ctl** scenario results from the plant absorption and not the soil fluxes (see Fig. S9). The soil fluxes have a small diurnal variability, although on average, the soil flux becomes slightly less negative during the day when the abiotic production term increases with growing temperature (Abadie et al., 2022). The use of the biosphere fluxes from the ORCHIDEE LSM instead of the SIB 4 LSM leads to the same conclusion (see Fig. S10).

To conclude, the diurnal rectifier effect for COS can be neglected when performing forward and inverse modelling studies. This conclusion must be qualified considering the fact that the plant uptake is underestimated in the two LSMs (Kooijmans et al., 2021, Maignan et al., 2021) and that the long-term rectifier effect was not completely assessed. Because of the memory cost of saving 3 hourly fluxes, we only performed one year of the **Diurnal** scenario. Multi-year simulations would allow an assessment of the effect of the rectifier effect on the mean latitudinal gradient (Denning et al., 1995)

4 Summary and conclusions

With the participation of seven transport models, a control case has been constructed to evaluate the state-of-the-art seasonal fluxes of COS while quantifying the transport errors, as another step to better constrain the COS global budget. We analyzed the concentrations of COS simulated by the atmospheric transport models at the location and time of surface and airborne campaign measurements. Specifically, we focused the analysis both on the model-to-model and the model-observations differences in:

1. Large-scale IH gradient, by comparing modeled and observed IH gradients of COS.
2. Simulated seasonal cycles, by comparing observed seasonal cycles at surface stations.
3. Vertical profiles of COS, by comparing modeled and observed vertical gradients of COS between the PBL and the free troposphere.

In addition, we quantified the sensitivity of the seasonal cycle and the latitudinal distribution of COS to a change in biosphere fluxes and to a change in oceanic fluxes. The diurnal rectifier effect has also been quantified on the seasonal cycle of COS by comparing the COS mixing ratios given by three-hourly fluxes and the COS mixing ratios given by monthly fluxes for the year 2015.

The main conclusions can be summarized as follows:
1. In regards to the mean seasonal cycle and the latitudinal distribution of COS mole fractions, the model spread in COS simulations is mainly caused by the subgrid-scale parameterisation (convective and boundary layer processes). However, in the vicinity of flux hot-spots, the model resolution becomes crucial.
2. The model spread in COS surface mixing ratios is the largest in summer in the northern high latitudes. The model spread at boreal sites can reach 70 ppt in summer, leading to divergences in seasonal amplitude of more than 50 ppt. The transport errors can potentially lead to significant uncertainties in the northern biosphere sink inferred through atmospheric inverse modeling using COS observations.
3. Overall, the difference between the modeled and observed COS values is larger than the model spread, pointing to incomplete knowledge of the COS budget, when using state-of-the-art component fluxes.
4. In agreement with earlier studies, model-observation comparisons emphasize the need of a missing tropical source, more biosphere uptake and likely smaller ocean emissions in the Northern Hemisphere summer, especially at high latitudes.
5. Based on airborne measurements over Northern America, models predict a positive vertical gradient between 1 and 4 km, while observations point to a negative gradient all year around, with a stronger gradient in late summer. This again points to the need for stronger COS uptake over Northern America.
6. Alternative flux combinations lead to similar conclusions. Indeed, the replacement of the biosphere flux simulated by the SIB4 LSM (Kooijmans et al., 2021) by the biosphere fluxes simulated by the ORCHIDEE LSM (Maignan et al., 2021; Abadie et al., 2022) in the **Ctl** scenario leads to minor change in mean seasonal cycle and IH gradient. Likewise, the replacement of the indirect ocean flux through DMS of Lana et al. (2011) by the ocean fluxes from Belviso et al. (2012) in the **Ctl** scenario has a minor impact under the assumption of a global constant conversion factor between DMS and COS (see discussion below).
7. The diurnal rectifier effect on the mean seasonal is negligible at most surface stations except at a few continental stations over Northern America where the diurnal rectifier effect does not exceed 30 ppt. This implies that the use of monthly biosphere fluxes instead of three-hourly biosphere fluxes is an acceptable simplification for COS budget studies. However, the assessment of the diurnal rectifier effect on the latitudinal distribution would require to perform the same experiment but over several years.

5 Discussion and future work

The atmospheric chemistry of COS was not included in the ATMs to isolate the transport errors. However, the chemistry related to COS remains poorly resolved. The current notion of the atmospheric chemistry of COS is that 100 $GgS.yr^{-1}$ is oxidized in the atmosphere and 50 $GgS.yr^{-1}$ is photolyzed in the stratosphere. Because of the small importance of these sources in the COS budget, their introduction in the ATMs is not expected to modify the conclusions of this study. A second assumption of this study is that the DMS emitted by the ocean is instantaneously oxidized into COS with a yield from Barnes et al. (1996). Recently, a **stable** intermediate from DMS oxidation, the hydroperoxymethyl thioformate (HPMTF), has been discovered to be the main precursor of COS (Jernigan et al., 2022). The introduction of this chemical pathway in an Atmospheric Chemistry Transport Model led to more COS emissions in the tropics but with a magnitude three times lower than the DMS fluxes used in this study (Jernigan et al., 2022). However, these results are still preliminary. If these reactions are confirmed by more chamber studies and observations in the future, the full chemistry of DMS and COS needs to be taken into account to accurately evaluate the state of the art COS fluxes.

This analysis, focused here on the mean seasonal cycle and the inter-hemispheric gradient, could be extended in the future to the inter-annual variations and the long term trend of the COS mixing ratios. The trend was not analysed because some inter-annual fluxes (e.g. anthropogenic) were not always available. Moreover, the COS mixing ratios derived from the atmospheric inversion of Ma et al. (2021) that was used to rescale the biosphere fluxes were climatological, which is not realistic in regards to the current decreasing trend of COS mole fraction since 2014 and its implication on biosphere fluxes (Belviso et al., 2022).

Finally, the sparse and uneven cover of the observations limits the evaluation of the COS fluxes to the footprint area of these stations. A complementary paper will also evaluate the COS fluxes using airborne measurements from the Atoms and HIAPER Pole-toPole Observations (HIPPO; Wofsy, 2011) campaigns. Although they are limited in time, these measurements will give additional insight to the COS fluxes over the tropical Atlantic and Pacific Ocean. Satellites offer the perspective of constraining the tropical areas over long periods of time (Glattor et al., 2015; Stinecipher et al., 2022, Vincent and Dhunia, 2017), but the retrievals still entail large uncertainties (Whelan et al., 2018; Serio et al., 2021). The complementary paper will evaluate the fluxes of COS at several FTIR stations and will quantify the transport errors.

Annexe: Additional transport model description

LMDz

The LMDz ATM has a spatial resolution of 3.75° × 1.9° (longitude times latitude) with 39 layers in the vertical, based on the general circulation model developed at the Laboratoire de Météorologie Dynamique, LMDz (Hourdin et al., 2020). LMDz6A is our reference version: it was prepared for the 6th Climate Intercomparison Project (CMIP6) as part of the Institut Pierre-Simon Laplace Earth system model. We use the offline version of the LMDz code, which was created by Hourdin and Armengaud (1999) and adapted by Chevallier et al. (2005) for atmospheric inversion. It is driven by air mass fluxes calculated by the complete general circulation model, run at the same resolution and nudged here towards winds from the fifth generation of meteorological analyses of the European Centre for Medium-Range Weather Forecasts (ECMWF) (ERA5). The off-line model only solves the mass balance equation for tracers, which significantly reduces the computation time. This LMDz version recently participated in the TRANSCOM experiment for CO_2 weather (Zhang et al., 2022).

TM5

TM5 is the global chemistry Transport Model, version 5 (TM5) (Krol et al., 2005). It allows two-way nested zooming and is specifically useful for multiple-resolution zooming modeling of trace gases in troposphere and stratosphere. The earlier version of TM5 is the parent TM3 model, which was originally developed by Heimann et al. (1988) and has been widely used in global atmospheric chemistry studies. TM5 is designed for tracer models and it is used extensively in inversion studies for various trace gases, e.g., CO, CO_2, CH_4 and COS. In this study, we used the forward-mode of TM5-4DVAR for COS at a high resolution of 2° × 2° with vertically 25 layers.

MIROC4

MIROC4-ACTM is a new generation Model for Interdisciplinary Research on Climate (MIROC, version 4.0) based atmospheric chemistry-transport model (Patra et al., 2018). The horizontal triangular truncation at a total horizontal wave number of 42 (T42; latitude and longitude ~2.81 × 2.81°) is used in the present study. MIROC4-ACTM has the fully resolved stratosphere and mesosphere by implementing the hybrid vertical coordinate of pressure-sigma (surface to about the tropopause) and pressure (about 300 hPa and above). The MIROC4-ACTM has a spectral dynamical core and uses a flux-form semi-Lagrangian scheme for the tracer advection (Lin and Rood 1996). The radiative transfer scheme considers 37 absorption bands, consisting of 23 in the visible and ultraviolet regions enabling better representation of photolysis for chemical species (Sekiguchi and Nakajima, 2008). The cumulus convection scheme is based on Arakawa and Schubert (1974), in which cloud base mass flux is treated as a prognostic variable. The sub-grid vertical mixing is parameterized based on the level 2 scheme of the turbulence closure (Mellor and Yamada 1982). The model participated in various model intercomparison projects, e.g., TransCom-air of air (Krol et al., 2018), and flux inversions are performed for CO_2, CH_4 and N_2O (Chandra et al., 2021a,b; Patra et al., 2022) which have contributed to various international emission and removal budget assessments.

TOMCAT

TOMCAT/SLIMCAT is a global 3-D off-line chemical transport model (Chipperfield, 2006). It is used to study a range of chemistry-aerosol-transport issues in the troposphere and stratosphere. The model is usually forced by ECMWF meteorological (re)analyses, although GCM output can also be used. When using ECMWF fields, as in the experiments described here, the model reads in the 6-hourly fields of temperature, humidity, vorticity, divergence and surface pressure. The resolved vertical motion is calculated online from the vorticity. Tracer advection is performed using the conservation of second-order moments scheme of Prather (1986). For the experiments described here the model was run at horizontal resolution of 2.8° × 2.8° with 60 hybrid σ-pressure levels from the surface to ~60 km. The model was forced by ECMWF ERA-Interim reanalyses (Dee et al., 2011). Convective mass fluxes were also taken from ERA-Interim reanalyses and mixing in the boundary layer is based on the scheme of Louis (1979), as described in Stockwell and Chipperfield (1999).

NICAM-TM

NICAM-TM is an atmospheric transport model based on Nonhydrostatic Icosahedral Atmospheric Model (NICAM: Satoh et al. 2014), which has an icosahedral grid system. The mean grid interval is 223 km and 112 km for “glevel-5” and “glevel-6”, respectively. Both the horizontal resolutions have the same vertical layer, whose number is 40 and the model top is approximately 45 km. Although NICAM-TM has on-line and off-line modes for atmospheric calculations, the off-line mode (Niwa et al., 2017) is used in this study, whose meteorological data are derived from an on-line NICAM-TM calculation with horizontal wind nudging. During both off-line and on-line calculations, mass conservation is achieved without any numerical mass fixer (Niwa et al. 2011, 2017). Using NICAM-TM, several inverse analyses of greenhouse gases have been performed (e.g., Niwa et al., 2021).

Acknowledgments

This study was funded by the CO2 Human Emissions (CHE) project, which received funding from the European Union’s Horizon 2020 research and innovation programme under grant agreement no. 776186. PKP and YN are partially supported by the Environmental Research and Technology Development Fund (JPMEERF21S20800) of the Environmental Restoration and Conservation Agency provided by the Ministry of Environment of Japan. YN is also supported by JSPS KAKENHI Grant Number JP22H05006. The simulations of NICAM-TM were performed by using the supercomputer system of NIES (SX-Aurora TSUBASA). The surface measurements from the NOAA network have been performed by scientists affiliated with NOAA (Stephen Montzka, Carolina Siso, John B. Miller, Fred Moore). Dan Yakir facilitates the collection of flask samples at WIS.

Open Research

The LMDz model is available from http://svn.lmd.jussieu.fr/LMDZ/LMDZ6/ under the CeCILL v2 free software license. The COS time series at station GIF from 2014 to 2019 are provided by Sauveur Belviso and can be downloaded from https://sharebox.lsce.ipsl.fr/index.php/s/Yxbj6dZsrc6nsOZ?path=2FGIF-observations (last access: 22 August 2022).

References

Abadie, C., Maignan, F., Remaud, M., Ogée, J., Campbell, J. E., Whelan, M. E., Kitz, F., Spielmann, F. M., Wohlfahrt, G., Wehr, R., Sun, W., Raoult, N., Seibt, U., Hauglustaine, D., Lennartz, S. T., Belviso, S., Montagne, D., and Peylin, P.: Global modelling of soil carbonyl sulfide exchanges, *Biogeosciences*, 19, 2427–2463, https://doi.org/10.5194/bg-19-2427-2022, 2022.

A. Anav, P. Friedlingstein, M. Kidston, L. Bopp, P. Ciais, et al.. Evaluating the land and ocean components of the global carbon cycle in the CMIP5 earth system models. *Journal of Climate*, American Meteorological Society, 2013, 26 (18), pp.6801-6843. ff10.1175/JCLI-D-12-00417.1ff. ffhal02929534f

Arakawa, A., and W. H. Schubert, 1974: Interactions of cumulus cloud ensemble with the large-scale environment, Part I. *J. Atmos. Sci.*, 31, 674−701. https://doi.org/10.1175/1520-0469(1974)031<0674:IOACCE>2.0.CO;2

Peter Bechtold, Noureddine Semane, Philippe Lopez, Jean-Pierre Chaboureau, Anton Beljaars, et al.. Representing Equilibrium and Nonequilibrium Convection in Large-Scale Models. *Journal of the Atmospheric Sciences*, American Meteorological Society, 2014, 71, pp.734-753. ff10.1175/JAS-D-13- 0163.1ff. ffhal-01065449f

Barnes, I., Becker, K. H., and Patroescu, I.: FTIR product study of the OH initiated oxidation of dimethyl sulphide: Observation of carbonyl sulphide and dimethyl sulphoxide, *Atmos. Environ*., 30, 1805–1814, https://doi.org/10.1016/1352-2310(95)00389-4, 1996.

Belviso, S., Masotti, I., Tagliabue, A., Bopp, L., Brockmann, P., Fichot, C., Caniaux, G., Prieur, L., Ras, J., Uitz, J., Loisel, H., Dessailly, D., Alvain, S., Kasamatsu, N., and Fukuchi, M.: DMS dynamics in the most oligotrophic subtropical zones of the global ocean, *Biogeochemistry*, 110, 215–241, https://doi.org/10.1007/s10533-011-9648-1, 2012.

Belviso, S., Lebegue, B., Ramonet, M., Kazan, V., Pison, I., Berchet, A., Delmotte, M., Yver-Kwok, C., Montagne, D., and Ciais, P.: A top-down approach of sources and non-photosynthetic sinks of carbonyl sulfide from atmospheric measurements over multiple years in the Paris region (France), *PLOS ONE*, 15, e0228419, https://doi.org/10.1371/journal.pone.0228419, 2020.

Belviso, S.; Remaud, M.; Abadie, C.; Maignan, F.; Ramonet, M.; Peylin, P. Ongoing Decline in the Atmospheric COS Seasonal Cycle Amplitude over Western Europe: Implications for Surface Fluxes. *Atmosphere* 2022, 13, 812. https://doi.org/10.3390/atmos13050812

Berry, J., Wolf, A., Campbell, J. E., Baker, I., Blake, N., Blake, D., Denning, A. S., Kawa, S. R., Montzka, S. A., Seibt, U., Stimler, K., Yakir, D., and Zhu, Z.: A coupled model of the global cycles of carbonyl sulfide and CO_2: A possible new window on the carbon cycle, *J. Geophys. Res.-Biogeo.*, 118, 842–852, https://doi.org/10.1002/jgrg.20068, 2013a.

Blake, N. J., Campbell, J. E., Vay, S. A., Fuelberg, H. E., Huey, L. G., Sachse, G., Meinardi, S., Beyersdorf, A., Baker, A., Barletta, B., Midyett, J., Doezema, L., Kamboures, M., McAdams, J., Novak, B., Rowland, F. S., and Blake, D. R.: Carbonyl sulfide (OCS): Large-scale distributions over North America during INTEX-NA and relationship to CO_2, *J. Geophys. Res.-Atmos.*, 113, D09S90, https://doi.org/10.1029/2007JD009163, 2008.

Campbell, J. E., Carmichael, G. R., Chai, T., Mena-Carrasco, M., Tang, Y., Blake, D. R., Blake, N. J., Vay, S. A., Collatz, G. J., Baker, I., Berry, J. A., Montzka, S. A., Sweeney, C., Schnoor, J. L., and Stanier, C. O.: Photosynthetic Control of Atmospheric Carbonyl Sulfide During the Growing Season, *Science*, 322, 1085–1088, https://doi.org/10.1126/science.1164015, 2008.

Campbell, J. E., Whelan, M. E.,Seibt, U., Smith, S. J., Berry, J. A., and Hilton, T. W.: Atmospheric carbonyl sulfide sources from anthropogenic activity: Implications for carbon cycle constraints, *Geophys. Res. Lett.*, 42, 3004–3010, https://doi.org/10.1002/2015GL063445, 2015.

Chandra, N., P. K. Patra, J. S. H. Bisht, A. Ito, T. Umezawa, S. Morimoto, S. Aoki, G. Janssens-Maenhout, R. Fujita, M. Takigawa, S. Watanabe, N. Saitoh, and J.G. Canadell, 2021: Emissions from the oil and gas sectors, coal mining and ruminant farming drive methane growth over the past three decades. *J. Meteor. Soc. Japan*, 99, 309-337. https://doi.org/10.2151/jmsj.2021-015

Chandra, N., Patra, P. K., Niwa, Y., Ito, A., Iida, Y., Goto, D., Morimoto, S., Kondo, M., Takigawa, M., Hajima, T., and Watanabe, M.: Estimated regional CO2 flux and uncertainty based on an ensemble of atmospheric CO2 inversions, *Atmos. Chem. Phys*. Discuss. [preprint], https://doi.org/10.5194/acp-2021-1039, in review, 2021.

F. Chevallier, M. Fisher, Philippe Peylin, S. Serrar, P. Bousquet, et al.. Inferring CO2 sources and sinks from satellite observations: Method and application to TOVS data. *Journal of Geophysical Research: Atmospheres*, American Geophysical Union, 2005, 110, pp.D24309. ff10.1029/2005JD006390ff. ffbioemco-00175976f

Chikira, M. and Sugiyama, M.: A Cumulus Parameterization with State-Dependent Entrainment Rate. Part I: Description and Sensitivity to Temperature and Humidity Profiles, *J. Atmos. Sci.*, 67, 2171–2193, doi:10.1175/2010JAS3316.1, 2010.

Chipperfield, M. P.: New version of the TOMCAT/SLIMCAT off-line chemical transport model: Intercomparison of stratospheric tracer experiments, *Q. J. Roy. Meteorol. Soci.*, 132, 1179–1203, 2006.

Commane, R., Meredith, L. K., Baker, I. T., Berry, J. A., Munger, J. W., Montzka, S. A., Templer, P. H., Juice, S. M., Zahniser, M. S., and Wofsy, S. C.: Seasonal fluxes of carbonyl sulfide in a midlatitude forest, *P. Natl. Acad. Sci*. USA, 112, 14162–14167, https://doi.org/10.1073/pnas.1504131112, 2015.

Dee, D. P., Uppala, S. M., Simmons, A. J., Berrisford, P., Poli, P., Kobayashi, S., Andrae, U., Balmaseda, M. A., Balsamo, G., Bauer, P., Bechtold, P., Beljaars, A. C. M., van de Berg, L., Bidlot, J., Bormann, N., Delsol, C., Dragani, R., Fuentes, M., Geer, A. J., Haimberger, L., Healy,

S. B., Hersbach, H., Hólm, E. V., Isaksen, L., Kållberg, P., Köhler, M., Matricardi, M., McNally, A. P., Monge-Sanz, B. M., Morcrette, J.-J., Park, B.-K., Peubey, C., de Rosnay, P., Tavolato, C., Thépaut, J.-N., and Vitart, F.: The ERA-Interim reanalysis: configuration and performance of the data assimilation system, *Q. J. Roy. Meteor. Soc.*, 137, 553–597, https://doi.org/10.1002/qj.828, 2011.

Denning, A. S., Fung, I. Y., and Randall, D.: Latitudinal gradient of atmospheric CO2 due to seasonal exchange with land biota, *Nature*, 376, 240–243, https://doi.org/10.1038/376240a0, 1995.

Denning, A. S., Taro Takahashi & Pierre Friedlingstein (1999) Can a strong atmospheric CO2 rectifier effect be reconciled with a “reasonable” carbon budget?, *Tellus B: Chemical and Physical Meteorology*, 51:2, 249-253, DOI: 10.3402/tellusb.v51i2.16277

Emanuel, K. A.: A Scheme for Representing Cumulus Convection in Large-Scale Models, *J. Atmos. Sci.*, 48, 2313–2329, https://doi.org/10.1175/1520-0469(1991)048<_x0032_313:ASFRCC>2.0.CO;2, 1991.

Glatthor, N., Höpfner, M., Baker, I. T., Berry, J., Campbell, J. E., Kawa, S. R., Krysztofiak, G., Leyser, A., Sinnhuber, B.-M., Stiller, G. P., Stinecipher, J., and Clarmann, T. V.: Tropical sources and sinks of carbonyl sulfide observed from space, *Geophys. Res. Lett.,* 42, 10082–10090, https://doi.org/10.1002/2015GL066293, 2015.

Goldan, P. D., Fall, R., Kuster, W. C., and Fehsenfeld, F.C.: Uptake of COS by growing vegetation: A major tropospheric sink, *J. Geophys. Res.-Atmos.*, 93, 14186–14192, https://doi.org/10.1029/JD093iD11p14186, 1988.

Grandpeix, J.-Y., Phillips, V. and Tailleux, R. (2004), Improved mixing representation in Emanuel's convection scheme. *Q.J.R. Meteorol. Soc.,* 130: 3207-3222. https://doi.org/10.1256/qj.03.144

Gurney, K. R., Law, R. M., Denning, A. S., Rayner, P. J., Baker, D., Bousquet, P., Bruhwiler, L., Chen, Y.-H., Ciais, P., Fan, S., Fung, I. Y., Gloor, M., Heimann, M., Higuchi, K., John, J., Maki, T., Maksyutov, S., Masarie, K., Peylin, P., Prather, M., Pak, B. C., Randerson, J., Sarmiento, J., Taguchi, S., Takahashi, T., and Yuen, C.-W.: Towards robust regional estimates of CO2 sources and sinks using atmospheric transport models, Nature, 415, 626– 630, https://doi.org/10.1038/415626a, 2002.

Heimann, M., Monfray, P., and Polian, G.: Long-range transport of 222Rn – a test for 3D tracer models, Chem. Geol., 70, 98–98, 1988.

Heimann M, Körner S. global atmospheric tracer model TM3: model description and user's manual; release 3.8 aThe. Technical Reports.2003(05).

Hoesly, R. M., Smith, S. J., Feng, L., Klimont, Z., Janssens-Maenhout, G., Pitkanen, T., Seibert, J. J., Vu, L., Andres, R. J., Bolt, R. M., Bond, T. C., Dawidowski, L., Kholod, N., Kurokawa, J.-I., Li, M., Liu, L., Lu, Z., Moura, M. C. P., O'Rourke, P. R., and Zhang, Q.: Historical (1750–2014) anthropogenic emissions of reactive gases and aerosols from the Community Emissions Data System (CEDS), Geosci. Model Dev., 11, 369–408, https://doi.org/10.5194/gmd-11-369-2018, 2018. a

Hirons LC, Inness P, Vitart F, Bechtold P. 2013. Understanding advances in the simulati on ofintraseasonal variability in the ECMWF model. Part II: The application of process-based diagnostics.Q. J. R.Meteorol. Soc.139: 1427 – 1444. DOI:10.1002/qj.2059.

Holtslag, A. A. M., & Moeng, C. -hoh. (1991). Eddy diffusivity and countergradient transport in the convective atmospheric boundary layer. *Journal Of The Atmospheric Sciences*, *48*, 1690-1698.doi:10.1175/1520-0469(1991)048<1690:EDACTI>2.0.CO;2

Hourdin, F. and Armengaud, A.: The use of finite-volume methods for atmospheric advection of trace species, Part I: Test of various formulations in a general circulation model, Mon. Weather Rev., 127, 822–837, doi:10.1175/1520- 0493(1999)127%3C0822:TUOFVM%3E2.0.CO;2, 1999.

Hourdin, F., Rio, C., Grandpeix, J.-Y., Madeleine, J.-B., Cheruy, F., Rochetin, N., et al. (2020). LMDZ6A: The atmospheric component of the IPSL climate model with improved and better tuned physics. *Journal of Advances in Modeling Earth Systems*, 12, e2019MS001892. https://doi.org/10.1029/2019MS001892

Hulswar, S., Simó, R., Galí, M., Bell, T. G., Lana, A., Inamdar, S., Halloran, P. R., Manville, G., and Mahajan, A. S.: Third revision of the global surface seawater dimethyl sulfide climatology (DMS-Rev3), Earth Syst. Sci. Data, 14, 2963–2987, https://doi.org/10.5194/essd-14-2963-2022, 2022.

Jernigan, C. M., Fite, C. H., Vereecken, L., Berkelhammer, M. B., Rollins, A. W., Rickly, P. S., et al. (2022). Efficient production of carbonyl sulfide in the low-NOx oxidation of dimethyl sulfide. *Geophysical Research Letters*, 49, e2021GL096838. https://doi.org/10.1029/2021GL096838

Kooijmans, L. M. J., Cho, A., Ma, J., Kaushik, A., Haynes, K. D., Baker, I., Luijkx, I. T., Groenink, M., Peters, W., Miller, J. B., Berry, J. A., Ogée, J., Meredith, L. K., Sun, W., Kohonen, K.-M., Vesala, T., Mammarella, I., Chen, H., Spielmann, F. M., Wohlfahrt, G., Berkelhammer, M., Whelan, M. E., Maseyk, K., Seibt, U., Commane, R., Wehr, R., and Krol, M.: Evaluation of carbonyl sulfide biosphere exchange in the Simple Biosphere Model (SiB4), Biogeosciences, 18, 6547–6565, https://doi.org/10.5194/bg-18-6547-2021, 2021.

Krol, M., Houweling, S., Bregman, B., van den Broek, M., Segers, A., van Velthoven, P., Peters, W., Dentener, F., and Bergamaschi, P.: The two-way nested global chemistry-transport zoom model TM5: algorithm and applications, Atmos. Chem. Phys., 5, 417–432, https://doi.org/10.5194/acp-5-417-2005, 2005.

Krol, M., de Bruine, M., Killaars, L., Ouwersloot, H., Pozzer, A., Yin, Y., Chevallier, F., Bousquet, P., Patra, P., Belikov, D., Maksyutov, S., Dhomse, S., Feng, W., and Chipperfield, M. P.: Age of air as a diagnostic for transport timescales in global models, Geosci. Model Dev., 11, 3109–3130, https://doi.org/10.5194/gmd-11-3109-2018, 2018.

Kuai, L., Worden, J. R., Campbell, J. E., Kulawik, S. S., Li, K.-F., Lee, M., Weidner, R. J., Montzka, S. A., Moore, F. L., Berry, J. A., Baker, I., Denning, A. S., Bian, H., Bowman, K. W., Liu, J., and Yung, Y. L.: Estimate of carbonyl sulfide tropical oceanic surface fluxes using Aura Tropospheric Emission Spectrometer observations, J. Geophys. Res.-Atmos., 120, 11012–11023, https://doi.org/10.1002/2015JD023493, 2015.

Lana, A., Bell, T. G., Simó, R., Vallina, S. M., Ballabrera-Poy, J., Kettle, A. J., Dachs, J., Bopp, L., Saltzman, E. S., Stefels, J., Johnson, J. E., and Liss, P. S.: An updated climatology of surface dimethlysulfide concentrations and emission fluxes in the global ocean, Global Biogeochem. Cy., 25, GB1004, https://doi.org/10.1029/2010GB003850, 2011

Lana A, Simó R, Vallina SM, Dachs J (2012) Re-examination of global emerging patterns of ocean DMS concentration. Biogeochemistry 110:173–182.

Launois, T., Peylin, P., Belviso, S., and Poulter, B.: A new model of the global biogeochemical cycle of carbonyl sulfide – Part 2: Use of carbonyl sulfide to constrain gross primary productivity in current vegetation models, Atmos. Chem. Phys., 15, 9285–9312, https://doi.org/10.5194/acp-15-9285-2015, 2015b.

Law, R. M., Rayner, P. J., Denning, A. S., Erickson, D., Fung, I. Y., Heimann, M., Piper, S. C., Ramonet, M., Taguchi, S., Taylor, J. A., Trudinger, C. M., and Watterson, I. G.: Variations in modeled atmospheric transport of carbon dioxide and the consequences for CO2 inversions, Global Biogeochem. Cy., 10, 783– 796, https://doi.org/10.1029/96GB01892, 1996.

Leer, B. V.: Towards the ultimate conservative difference scheme, IV. A new approach to numerical convection, J. Comput. Phys., 23, 276–299, doi:10.1016/0021-9991(77)90095-X, 1977.

Lennartz, S. T., Marandino, C. A., von Hobe, M., Cortes, P., Quack, B., Simo, R., Booge, D., Pozzer, A., Steinhoff, T., ArevaloMartinez, D. L., Kloss, C., Bracher, A., Röttgers, R., Atlas, E., and Krüger, K.: Direct oceanic emissions unlikely to account for the missing source of atmospheric carbonyl sulfide, Atmos. Chem. Phys., 17, 385–402, https://doi.org/10.5194/acp-17-385- 2017, 2017.

Lennartz, S. T., Gauss, M., von Hobe, M., and Marandino, C. A.: Monthly resolved modelled oceanic emissions of carbonyl sulphide and carbon disulphide for the period 2000–2019, Earth Syst. Sci. Data, 13, 2095–2110, https://doi.org/10.5194/essd-13- 2095-2021, 2021a.

Lennartz, S. T., Marandino, C. A., von Hobe, M., Andreae, M. O., Aranami, K., Atlas, E., Berkelhammer, M., Bingemer, H., Booge, D., Cutter, G., Cortes, P., Kremser, S., Law, C. S., Marriner, A., Simó, R., Quack, B., Uher, G., Xie, H., and Xu, X.: Marine carbonyl sulfide (OCS) and carbon disulfide (CS2): a compilation of measurements in seawater and the marine boundary layer, Earth Syst. Sci. Data, 12, 591–609, https://doi.org/10.5194/essd12-591-2020, 2020b.

Lin, X., Ciais, P., Bousquet, P., Ramonet, M., Yin, Y., Balkanski, Y., Cozic, A., Delmotte, M., Evangeliou, N., Indira, N. K., Locatelli, R., Peng, S., Piao, S., Saunois, M., Swathi, P. S., Wang, R., Yver-Kwok, C., Tiwari, Y. K., and Zhou, L.: Simulating CH_4 and CO_2 over South and East Asia using the zoomed chemistry transport model LMDz-INCA, Atmos. Chem. Phys., 18, 9475–9497, https://doi.org/10.5194/acp-18-9475-2018, 2018.

Lin, J.-L., Kiladis, G. N., Mapes, B. E., Weickmann, K. M., Sperber, K. R., Lin, W., Wheeler, M. C., Schubert, S. D., Del Genio, A., Donner, L. J., Emori, S., Gueremy, J.-F., Hourdin, F., Rasch, P. J., Roeckner, E., and Scinocca, J. F.: Tropical Intraseasonal Variability in 14 IPCC AR4 Climate Models. Part I: Convective Signals, J. Climate, 19, 2665–2690, https://doi.org/10.1175/JCLI3735.1, 2006.

Lin, S.-J., and R. Rood, 1996: Multidimensional flux-form semi- Lagrangian transport schemes. Mon. Wea. Rev., 124, 2046− 2070. https://doi.org/10.1175/1520-0493(1996)124<2046:MFFSLT>2.0.CO;2

Locatelli, R., Bousquet, P., Hourdin, F., Saunois, M., Cozic, A., Couvreux, F., Grandpeix, J.-Y., Lefebvre, M.-P., Rio, C., Bergamaschi, P., Chambers, S. D., Karstens, U., Kazan, V., van der Laan, S., Meijer, H. A. J., Moncrieff, J., Ramonet, M., Scheeren, H. A., Schlosser, C., Schmidt, M., Vermeulen, A., and Williams, A. G.: Atmospheric transport and chemistry of trace gases in LMDz5B: evaluation and implications for inverse modelling, Geosci. Model Dev., 8, 129–150, https://doi.org/10.5194/gmd-8- 129-2015, 2015a.

Louis, J.-F., A parametric model of vertical eddy fluxes in the atmosphere, Boundary Layer Meteorok, 17, 187-202,1979.

Ma, J., Kooijmans, L. M. J., Cho, A., Montzka, S. A., Glatthor, N., Worden, J. R., Kuai, L., Atlas, E. L., and Krol, M. C.: Inverse modelling of carbonyl sulfide: implementation, evaluation and implications for the global budget, Atmos. Chem. Phys., 21, 3507–3529, https://doi.org/10.5194/acp-21-3507-2021, 2021.

Maignan, F., Abadie, C., Remaud, M., Kooijmans, L. M. J., Kohonen, K.-M., Commane, R., Wehr, R., Campbell, J. E., Belviso, S., Montzka, S. A., Raoult, N., Seibt, U., Shiga, Y. P., Vuichard, N., Whelan, M. E., and Peylin, P.: Carbonyl sulfide: comparing a mechanistic representation of the vegetation uptake in a land surface model and the leaf relative uptake approach, Biogeosciences, 18, 2917–2955, https://doi.org/10.5194/bg-18- 2917-2021, 2021.

Mellor, G. L. and Yamada, T.: A Hierarchy of Turbulence Closure Models for Planetary Boundary Layers, J. Atmos. Sci., 31, 1791– 1806, 1974.

Mellor, G. L., and T. Yamada, 1982: Development of a turbulence closure model for geostrophic fluid problems. Rev. Geophys., 20, 851−875. https://doi.org/10.1029/RG020i004p00851

Meredith, L. K., Boye, K., Youngerman, C., Whelan, M., Ogée, J., Sauze, J., and Wingate, L.: Coupled Biological and Abiotic Mechanisms Driving Carbonyl Sulfide Production in Soils, Soil Systems, 2, 37, https://doi.org/10.3390/soilsystems2030037, 2018.

Miura, H.: An Upwind-Biased Conservative Advection Scheme for Spherical Hexagonal–Pentagonal Grids, Mon. Weather Rev., 135, 4038–4044, doi:10.1175/2007MWR2101.1, 2007.

Montzka, S. A., Calvert, P., Hall, B. D., Elkins, J. W., Conway, T. J., Tans, P. P., and Sweeney, C.: On the global distribution, seasonality, and budget of atmospheric carbonyl sulfide (COS) and some similarities to CO2, J. Geophys. Res.-Atmos., 112, D09302, https://doi.org/10.1029/2006JD007665, 2007.

Nakanishi, M. and Niino, H.: An Improved Mellor–Yamada Level-3 Model with Condensation Physics: Its Design and Verification, Bound.-Lay. Meteorol., 112, 1–31, doi:10.1023/B:BOUN.0000020164.04146.98, 2004.

Niwa, Y., Tomita, H., Satoh, M., and Imasu, R.: A Three-Dimensional Icosahedral Grid Advection Scheme Preserving Monotonicity and Consistency with Continuity for Atmo- spheric Tracer Transport, J. Meteorol. Soc. Jpn., 89, 255–268, doi:10.2151/jmsj.2011-306, 2011.

Niwa, Y., Tomita, H., Satoh, M., Imasu, R., Sawa, Y., Tsuboi, K., Matsueda, H., Machida, T., Sasakawa, M., Belan, B., and Saigusa, N.: A 4D-Var inversion system based on the icosahedral grid model (NICAM-TM 4D-Var v1.0) – Part 1: Offline forward and adjoint transport models, Geosci. Model Dev., 10, 1157–1174, https://doi.org/10.5194/gmd-10-1157-2017, 2017.

Niwa, Y., Sawa, Y., Nara, H., Machida, T., Matsueda, H., Umezawa, T., Ito, A., Nakaoka, S.-I., Tanimoto, H., and Tohjima, Y.: Estimation of fire-induced carbon emissions from Equatorial Asia in 2015 using in situ aircraft and ship observations, Atmos. Chem. Phys., 21, 9455–9473, https://doi.org/10.5194/acp-21-9455-2021, 2021.

Ogée, J., Sauze, J., Kesselmeier, J., Genty, B., Van Diest, H., Launois, T., and Wingate, L.: A new mechanistic framework to predict OCS fluxes from soils, Biogeosciences, 13, 2221–2240, https://doi.org/10.5194/bg-13-2221-2016, 2016.

Parazoo, N. C., Bowman, K. W., Baier, B. C., Liu, J., Lee, M., Kuai, L., et al. (2021). Covariation of airborne biogenic tracers (CO_2, COS, and CO) supports stronger than expected growing season photosynthetic uptake in the southeastern US. *Global Biogeochemical Cycles*, 35, e2021GB006956. https://doi.org/10.1029/2021GB006956

Parazoo, N. C., Denning, A. S., Berry, J. A., Wolf, A., Randall, D. A., Kawa, S. R., Pauluis, O., and Doney, S. C.: Moist synoptic transport of CO_2 along the mid-latitude storm track, Geophys. Res. Lett., 38, L09804, https://doi.org/10.1029/2011GL047238, 2011.

Patra, P. K., et al. (2011a), TransCom model simulations of CH4 and related species: Linking transport, surface flux and chemical loss with CH4 variability in the troposphere and lower stratosphere, Atmos. Chem. Phys., 11, 12,813–12,837, doi:10.5194/acp-11-12813-2011.

Patra, P. K., Takigawa, M., Watanabe, S., Chandra, N., Ishijima, K., & Yamashita, Y. (2018). Improved Chemical Tracer Simulation by MIROC4.0-based Atmospheric Chemistry-Transport Model (MIROC4-ACTM). SOLA, 14, 91–96. https://doi.org/10.2151/sola.2018-016

Patra, P., E. Dlugokencky, J. Elkins, G. Dutton, Y. Tohjima, M. Sasakawa, A. Ito, R. Weiss, M. Manizza, P. Krummel, R. Prinn, S. O'Doherty, D. Bianchi, C. Nevison,E. Solazzo, H. Lee, S. Joo, E. Kort, S. Maity, and M. Takigawa (2022). Forward and inverse modelling of atmospheric nitrous oxide using MIROC4-atmospheric chemistry-transport model. Journal of the Meteorological Society of Japan. Ser. II, 100 (2), in press. https://doi.org/10.2151/jmsj.2022-018.

Prather, M.: Numerical advection by conservation of 2nd order moments, J. Geophys. Res., 91, 6671–6681,

doi:10.1029/JD091iD06p06671, 1986.

Protoschill-Krebs, G., Wilhelm, C., and Kesselmeier, J.: Consumption of carbonyl sulphide (COS) by higher plant carbonic anhydrase (CA), Atmos. Environ., 30, 3151–3156, https://doi.org/10.1016/1352-2310(96)00026-X, 1996.

Remaud, M., Chevallier, F., Cozic, A., Lin, X., and Bousquet, P.: On the impact of recent developments of the LMDz atmospheric general circulation model on the simulation of CO_2 transport, Geosci. Model Dev., 11, 4489–4513, https://doi.org/10.5194/gmd-11-4489-2018, 2018.

Remaud, M., Chevallier, F., Maignan, F., Belviso, S., Berchet, A., Parouffe, A., Abadie, C., Bacour, C., Lennartz, S., and Peylin, P.: Plant gross primary production, plant respiration and carbonyl sulfide emissions over the globe inferred by atmospheric inverse modelling, Atmos. Chem. Phys., 22, 2525–2552, https://doi.org/10.5194/acp-22-2525-2022, 2022.

Rio, C. and Hourdin, F.: A Thermal Plume Model for the Convective Boundary Layer: Representation of Cumulus Clouds, J. Atmos. Sci., 65, 407–425, https://doi.org/10.1175/2007JAS2256.1, 2008.

Rochetin, N., Grandpeix, J.-Y., Rio, C., and Couvreux, F.: Deep Convection Triggering by Boundary Layer Thermals. Part II: Stochastic Triggering Parameterization for the LMDZ GCM, J. Atmospheric Sciences, 71, 515–538, https://doi.org/10.1175/JAS-D-12-0337.1, 2013.

Russell, G.L., and J.A. Lerner, 1981: A new finite-differencing scheme for tracer transport equation. J. Appl. Meteorol., **20**, 1483-1498, doi:10.1175/1520-0450(1981)020<1483:ANFDSF>2.0.CO;2.

Saito, R., Patra, P. K., Sweeney, C., Machida, T., Krol, M., Houweling, S., Bousquet, P., Agusti-Panareda, A., Belikov, D., Bergmann, D., Bian, H., Cameron-Smith, P., Chipperfield, M. P., Fortems-Cheiney, A., Fraser, A., Gatti, L. V., Gloor, E., Hess, P., Kawa, S. R., Law, R. M., Locatelli, R., Loh, Z., Maksyutov, S., Meng, L., Miller, J. B., Palmer, P. I., Prinn, R. G., Rigby, M., and Wilson, C.: TransCom model simulations of methane: Comparison of vertical profiles with aircraft measurements, J. Geophys. Res.-Atmos., 118, 3891–3904, https://doi.org/10.1002/jgrd.50380, 2013.

Satoh, M., Tomita, H., Yashiro, H., Miura, H., Kodama, C., Seiki, T., Noda, A. T., Yamada, Y., Goto, D., Sawada, M., Miyoshi, T., Niwa, Y., Hara, M., Ohno, T., Iga, S., Arakawa, T., Inoue, T., and Kubokawa, H.: The Non-hydrostatic Icosahedral Atmo- spheric Model: description and development, Progress in Earth and Planetary Science, 1, 1–32, doi:10.1186/s40645-014-0018-1, 2014.

Stockwell, D. Z. and Chipperfield, M. P.: A tropospheric chemical-transport model: Development and validation of the model transport schemes, Q. J. Roy. Meteorol. Soc., 125, 1747–1783, 1999.

Sekiguchi, M., and T. Nakajima, 2008: A k-distribution based radiation code and its computational optimization for an atmospheric general circulation model. J. Quant. Spectrosc. Radiat. Transfer, 109, 2779–2793. https://doi.org/10.1016/j.jqsrt.2008.07.013

Serio, C., Masiello, G., Mastro, P., Belviso, S., and Remaud, M.: Seasonal variability of degrees of freedom and its effect over time series and spatial patterns of atmospheric gases from satellite: application to carbonyl sulfide (OCS), Remote Sensing of Clouds and the Atmosphere XXVI, 11859, 11–23, https://doi.org/10.1117/12.2599761, 2021.

Stinecipher, J. R., Cameron-Smith, P. J., Blake, N. J., Kuai, L., Lejeune, B., Mahieu, E., Simpson, I. J., and Campbell, J. E.: Biomass Burning Unlikely to Account for Missing Source of Carbonyl Sulfide, Geophys. Res. Lett., 46, 14912–14920, https://doi.org/10.1029/2019GL085567, 2019.

Stinecipher, J. R., Cameron-Smith, P., Kuai, L., Glatthor, N., Höpfner, M., Baker, I., et al. (2022). Remotely sensed carbonyl sulfide constrains model estimates of Amazon primary productivity. *Geophysical Research Letters*, 49, e2021GL096802. https://doi.org/10.1029/2021GL096802

Stockwell, D.Z. and Chipperfield, M.P. (1999), A tropospheric chemical-transport model: Development and validation of the model transport schemes. Q.J.R. Meteorol. Soc., 125: 1747-1783. https://doi.org/10.1002/qj.49712555714

Suntharalingam, P., Kettle, A. J., Montzka, S. M., and Jacob, D. J.: Global 3-D model analysis of the seasonal cycle of atmospheric carbonyl sulfide: Implications for terrestrial vegetation uptake, Geophys. Res. Lett., 35, L19801, https://doi.org/10.1029/2008GL034332, 2008.

Sweeney, C., Karion, A., Wolter, S., Newberger, T., Guenther, D., Higgs, J. A., Andrews, A. E., Lang, P. M., Neff, D., Dlugokencky, E., Miller, J. B., Montzka, S. A., Miller, B. R., Masarie, K. A., Biraud, S. C., Novelli, P. C., Crotwell, M., Crotwell, A. M., Thoning, K., and Tans, P. P.: Seasonal climatology of CO2 across North America from aircraft measurements in the NOAA/ESRL Global Greenhouse Gas Reference Network, J. Geophys. Res.-Atmos., 120, 5155–5190, https://doi.org/10.1002/2014JD022591, 2015.

Thoning, K. W., Tans, P. P., and Komhyr, W. D.: Atmospheric carbon dioxide at Mauna Loa Observatory: 2. Analysis of the NOAA GMCC data, 1974–1985, J. Geophys. Res.-Atmos., 94, 8549–8565, https://doi.org/10.1029/JD094iD06p08549, 1989

Tiedtke, M.: A Comprehensive Mass Flux Scheme for Cumulus Parameterization in Large-Scale Models, Mon. Wea. Rev., 117, 1779–1800, 1989.

Vesala, T., Kohonen, K.-M., Kooijmans, L. M. J., Praplan, A. P., Foltýnová, L., Kolari, P., Kulmala, M., Bäck, J., Nelson, D., Yakir, D., Zahniser, M., and Mammarella, I.: Long-term fluxes of carbonyl sulfide and their seasonality and interannual variability in a boreal forest, Atmos. Chem. Phys., 22, 2569–2584, https://doi.org/10.5194/acp-22-2569-2022, 2022.

Vincent, R. A. and Dudhia, A.: Fast retrievals of tropospheric carbonyl sulfide with IASI, Atmos. Chem. Phys., 17, 2981–3000, https://doi.org/10.5194/acp-17-2981-2017, 2017

Wang, Y., Deutscher, N. M., Palm, M., Warneke, T., Notholt, J., Baker, I., Berry, J., Suntharalingam, P., Jones, N., Mahieu, E., Lejeune, B., Hannigan, J., Conway, S., Mendonca, J., Strong, K., Campbell, J. E., Wolf, A., and Kremser, S.: Towards understanding the variability in biospheric CO2 fluxes: using FTIR spectrometry and a chemical transport model to investigate the sources and sinks of carbonyl sulfide and its link to CO2, Atmos. Chem. Phys., 16, 2123–2138, https://doi.org/10.5194/acp16-2123-2016, 2016.

Watanabe, S., H. Miura, M. Sekiguchi, T. Nagashima, K. Sudo, S. Emori, and M. Kawamiya, 2008: Development of an atmospheric general circulation model for integrated Earth system modeling on the Earth Simulator. J. Earth Simulator, 9, 27−35.

Whelan, M. E., Hilton, T. W., Berry, J. A., Berkelhammer, M., Desai, A. R., and Campbell, J. E.: Carbonyl sulfide exchange in soils for better estimates of ecosystem carbon uptake, Atmos. Chem. Phys., 16, 3711–3726, https://doi.org/10.5194/acp16-3711-2016, 2016.

Whelan, M. E., Lennartz, S. T., Gimeno, T. E., Wehr, R., Wohlfahrt, G., Wang, Y., Kooijmans, L. M. J., Hilton, T. W., Belviso, S., Peylin, P., Commane, R., Sun, W., Chen, H., Kuai, L., Mammarella, I., Maseyk, K., Berkelhammer, M., Li, K.-F., Yakir, D., Zumkehr, A., Katayama, Y., Ogée, J., Spielmann, F. M., Kitz, F., Rastogi, B., Kesselmeier, J., Marshall, J., Erkkilä, K.-M., Wingate, L., Meredith, L. K., He, W., Bunk, R., Launois, T., Vesala, T., Schmidt, J. A., Fichot, C. G., Seibt, U., Saleska, S., Saltzman, E. S., Montzka, S. A., Berry, J. A., and Campbell, J. E.: Reviews and syntheses: Carbonyl sulfide as a multi-scale tracer for carbon and water cycles, Biogeosciences, 15, 3625– 3657, https://doi.org/10.5194/bg-15-3625-2018, 2018.

Wofsy, S. C.: HIAPER Pole-to-Pole Observations (HIPPO): finegrained, global-scale measurements of climatically important atmospheric gases and aerosols, Philos. T. Roy. Soc. A, 369, 2073– 2086, https://doi.org/10.1098/rsta.2010.0313, 2011.

Wohlfahrt, G., Brilli, F., Hortnagl, L., Xu, X., Bingemer, H., Hansel, A. and Loreto, F. (2012), Carbonyl sulfide (COS) as a tracer for canopy photosynthesis, transpiration and stomatal conductance: potential and limitations. Plant, Cell & Environment, 35: 657-667. https://doi.org/10.1111/j.1365-3040.2011.02451.x

Zhang, L., Davis, K. J., Schuh, A. E., Jacobson, A. R., Pal, S., Cui, Y. Y., et al. (2022). Multi-season evaluation of CO_2 weather in OCO-2 MIP models. *Journal of Geophysical Research: Atmospheres*, 127, e2021JD035457. https://doi.org/10.1029/2021JD035457

Zumkehr, A., Hilton, T. W., Whelan, M., Smith, S., Kuai, L., Worden, J., and Campbell, J. E.: Global gridded anthropogenic emissions inventory of carbonyl sulfide, Atmos. Environ., 183, 11–19, https://doi.org/10.1016/j.atmosenv.2018.03.063, 2018.